Helsinki University of Technology Radio Laboratory Publications

Teknillisen korkeakoulun Radiolaboratorion julkaisuja

Espoo, May, 2001 REPORT S 247

SELECTED DEVELOPMENTS IN COMPUTATIONAL ELECTROMAGNETICS FOR RADIO ENGINEERING

Thesis for the degree of Doctor of Science in Technology

Jaakko Juntunen

TEKNILLINEN KORKEAKOULU
TEKNISKA HÖGSKOLAN
HELSINKI UNIVERSITY OF TECHNOLOGY
TECHNISCHE UNIVERSITÄT HELSINKI
UNIVERSITE DE TECHNOLOGIE D'HELSINKI

Helsinki University of Technology Radio Laboratory Publications
Teknillisen korkeakoulun Radiolaboratorion julkaisuja
Espoo, May 2001 REPORT S 247

SELECTED DEVELOPMENTS IN COMPUTATIONAL ELECTROMAGNETICS FOR RADIO ENGINEERING

Jaakko Juntunen

Dissertation for the degree of Doctor of Science in Technology to be presented with due permission for public examination and debate in Auditorium S4 at Helsinki University of Technology (Espoo, Finland) on the 26th of May 2001 at 12 o'clock noon.

Helsinki University of Technology
Department of Electrical and Communications Engineering
Radio Laboratory

Teknillinen korkeakoulu
Sähkö- ja tietoliikennetekniikan osasto
Radiolaboratorio

Preface

This thesis is based on work done at the Radio Laboratory of the Helsinki University of Technology during 1996-2000. Of that period, I spent the academic year 1998-1999 at the Aristotle University of Thessaloniki, Greece. I wish to express my gratitude to Professor Antti Räisänen, the supervisor of this work, for giving me the opportunity to work in Radio Laboratory and to find out the most suitable research topics in the fascinating area of computational radio engineering.

I want to express my gratitude to my coworkers at the Radio Laboratory and at the Aristotle University of Thessaloniki. Especially I want to mention Tommi Laitinen for good discussions during the course, Nikolaos Kantartzis and Ioannis Rekanos for proofreading some of my articles, Theodoros Kosmanis for helping in many practical arrangements in Thessaloniki, professor Theodoros Tsiboukis for making my stay in Thessaloniki possible at first place, Jani Ollikainen and Outi Kivekäs for suggesting and co-working the DRA simulation project, Riku Mäkinen for fruitful co-operation, Stina Lindberg and Marja Leppäharju for knowing and arranging everything, as secretaries always do. Every other fellow worker in the Radio Laboratory deserves also my sincere thanks for constituting a pleasant and open-minded working environment in the lab.

This research work is funded mostly by the Graduate School in Electronics, Telecommunications and Automation. This work has been financially supported also by Academy of Finland, Jenny and Antti Wihuri Foundation, Tekniikan Edistämissäätiö, TKK:n Tukisäätiö, European Union TMR grant number ERBFMBICT983462, Center of International Mobility (CIMO), HPY:n tutkimussäätiö, and Elektroniikkainsinöörien Säätiö, which are all gratefully acknowledged.

Finally, I use the opportunity to express my gratitude to my wife Mari, who took the risk to marry a numerician.

Espoo, January 2001

Jaakko Juntunen

Abstract

This thesis deals with the development and application of two simulation methods commonly used in radio engineering, namely the Finite-Difference Time-Domain method (FDTD) and the Finite Element Method (FEM). The main emphasis of this thesis is in FDTD.

FDTD has become probably the most popular computational technique in radio engineering. It is a well established, fairly accurate and easy-to-implement method. Being a time-domain method, it can provide wide-band information in a single simulation. It simulates physical wave propagation in the computational volume, and is thus especially useful for educational purposes and for gaining engineering insight into complicated wave interaction and coupling phenomena.

In this thesis, numerical dispersion taking place in the FDTD algorithm is analyzed, and a novel dispersion reduction procedure is described, based on artificial anisotropy. As a result, larger cells can be used to obtain the same accuracy in terms of dispersion error. Simulation experiments suggest that typically the dispersion reduction allows roughly doubling the cell size in each coordinate direction, without sacrificing the accuracy. The obtainable advantage is, however, dependent on the problem. In the open literature, a few other procedures are also presented to reduce the dispersion error. However, the rather dominating effect of unequal grid resolution along different coordinate directions has been neglected in previous studies.

The so-called Perfectly Matched Layer (PML) has proven to be a very useful absorbing boundary condition (ABC) in FDTD simulations. It is reliable, works well in wide frequency band and is easy to implement. The most notable deficiency of PML is that it enlarges the computational volume - in open 3-D structures easily by a factor of two. However, due to its advantages, PML has become a standard ABC. In this thesis, the operation of PML in FDTD has been studied theoretically, and some interesting properties of it not known before are uncovered. For example, it is shown that, surprisingly, PML can absorb perfectly (i.e. with zero reflection) plane waves propagating towards almost arbitrary given direction at given frequency. Optimizing the conductivity profile allows reduction of the PML thickness.

A typical application of the FDTD method is the design of a mobile handset antenna. An improved coaxial probe model has been developed for antenna simulations. The well-known resistive voltage source (RVS) model has also been discussed. A reference plane transformation is proposed to correct the simulated input impedance.

A popular thin-wire model in 2-D FDTD is discussed, and it is shown to be based on erroneous reasoning. The error has been corrected by a simple procedure, and the corrected model has been demonstrated to simulate infinite long thin wires much better than the commonly used model.

A novel way to implement singular basis functions in FEM is discussed. It is shown theoretically and demonstrated by examples that if a waveguide propagation mode contains field singularities, then explicit inclusion of singularities in finite element analysis is crucial in order to obtain accurate cut-off wavenumbers.

List of publications

This thesis is based on the work contained in the following papers:

[P1] **Jaakko Juntunen**, Theodoros D. Tsiboukis: Reduction of numerical dispersion in FDTD algorithm through artificial anisotropy. *IEEE Transactions on Microwave Theory and Techniques*, Vol. 48, No. 4, 2000, pp. 582-588.

[P2] **Jaakko Juntunen**, Nikolaos V. Kantartzis, Theodoros D. Tsiboukis: Zero reflection coefficient in discretized split-field PML. *IEEE Microwave and Wireless Components Letters*, Vol. 11, No. 4, 2001, pp. 155-157.

[P3] **Jaakko Juntunen**, Outi Kivekäs, Jani Ollikainen, Pertti Vainikainen: FDTD simulation of a wide-band half volume DRA. *Proceedings of the Fifth International Symposium on Antennas, Propagation and EM Theory (ISAPE 2000)*, Beijing, 2000, pp. 223-226.

[P4] **Jaakko Juntunen**: Note on the S_{11}-parameter and input impedance extraction in antenna simulations using FDTD. *Microwave and Optical Technology Letters*, Vol. 28, No. 1, 2001, pp. 8-11.

[P5] Riku Mäkinen, **Jaakko Juntunen**, Markku Kivikoski: An accurate 2D hard-source model for FDTD. *IEEE Microwave and Wireless Components Letters*, Vol. 11, No. 2, 2001, pp. 74-76.

[P6] **Jaakko Juntunen**, Theodoros D. Tsiboukis: On the FEM treatment of wedge singularities in waveguide problems. *IEEE Transactions on Microwave Theory and Techniques*, Vol. 48, No. 6, 2000, pp. 1030-1037.

Contribution of the author

Papers [P1,P4,P6] were mainly contributed by the author.

Paper [P2] was mainly contributed by the author, N.V. Kantartzis contributed to the introduction section.

Paper [P3] is a result of a collaboration work. The author is responsible of all simulations and numerical techniques presented in the paper, as well as the manuscript. Outi Kivekäs and Jani Ollikainen designed the prototypes and performed the measurements. The prototypes were manufactured in the mechanical workshop of the Radio Laboratory.

Paper [P5] is a result of a collaboration work. The initiative to this work is due to Riku Mäkinen, who discovered the inconsistency in the classical thin-wire formalism. The author proposed and realized a previously published [1] Green's function test to evaluate the effective radius of a wire model. Furthermore, the author suggested and realized the consistency comparisons between traditional and the proposed thin-wire models, using thin wire as a passive scattering structure. Riku Mäkinen performed the other tests and wrote the manuscript.

Other related papers authored or co-authored by this author are [O1-O7] listed in the reference list.

Contents

List of symbols and abbreviations

Symbols

a	aid variable
$a(\cdot,\cdot)$	bilinear form
B	byte
$\vec{B}$	magnetic flux density [T]
$\vec{B}_{new}$	updated value of magnetic flux density [T]
$\vec{B}_{old}$	old value of magnetic flux density before updating [T]
c	speed of light in medium [m/s]
c_0	speed of light in vacuum, $2.9979 \cdot 10^8$m/s
c_i	expansion coefficient
$\vec{D}$	electric flux density [C/m^2]
$(D_h u)_i$	approximation of derivative of u at a discrete point i
D_t	central-difference approximation of time-derivative
D_x	central-difference approximation of x-derivative
$d\vec{B}$	differential change of magnetic flux density [T]
dt	differential time increment [s]
$\vec{E}$	electric field intensity [V/m]
E_x	x-component of $\vec{E}$ [V/m]
E_y	y-component of $\vec{E}$ [V/m]
E_z	z-component of $\vec{E}$ [V/m]
F	representative field component
f	frequency [Hz], source function
f_c	cut-off frequency [Hz]
f_i	frequency as a design parameter in PML optimization [Hz]
f_w	bandwidth of a modulated Gaussian pulse [Hz]
f_0	center frequency of a modulated Gaussian pulse [Hz]
$\vec{H}$	magnetic field intensity [A/m]
H_x	x-component of $\vec{H}$ [A/m]
H_y	y-component of $\vec{H}$ [A/m]
H_z	z-component of $\vec{H}$ [A/m]
H_{zx}	x-part of split H_z in PML [A/m]
H_{zy}	y-part of split H_z in PML [A/m]
H_0	magnetic field intensity at a distance $\Delta/2$ from the axis of an infinite wire [A/m]
H^1	space of functions whose derivatives up to the first order are square integrable
h	edge length of a square cell [m], height of a monopole [mm]
i	integer index
$\vec{J}$	electric current density [A/m^2]
j	integer index, imaginary unit $\sqrt{-1}$

k	integer index, wavenumber [1/m]
k_x	x-component of wave vector [1/m]
k_y	y-component of wave vector [1/m]
k_z	z-component of wave vector [1/m]
L	linear operator
L_2	space of square-integrable functions
M	mega = multiplication factor 10^6
M	PML width parameter
N	width of a representative structure in cells, probe height in cells, number of basis functions in a finite element basis
n	integer index, conductivity profile exponent in PML
$O(a^b)$	remainder or error term of the order of a^b
P	aid parameter in PML reflection coefficient formula
p	time stepping order, order of finite element basis
Q	Courant-number in 1-D FDTD
Q_2	Courant-number in 2-D FDTD
Q_3	Courant-number in 3-D FDTD
R	resolution parameter
$R(\theta)$	theoretical reflection coefficient
R_2	resolution parameter in 2-D FDTD
$\hat{R}$	resolution parameter
r	distance to the origin in polar coordinates [m], distance to the z-axis in cylindrical coordinates [m], residual error function
r_i	radius of the inner conductor of a coaxial line [m]
r_o	radius of the outer conductor of a coaxial line [m]
S	pseudodifferential operator $c(\partial/\partial s)/(\partial/\partial t)$, aid parameter in PML reflection coefficient formula
S_i	aid parameter in PML reflection coefficient formula
S_{11}	return loss
s	generic coordinate direction x, y or z [m]
s_x	complex parameter in UPML
s_y	complex parameter in UPML
s_z	complex parameter in UPML
T	Gaussian pulse parameter, aid parameter in PML reflection coefficient formula
T_i	aid parameter in PML reflection coefficient formula
Ty	Turkel-Yefet -algorithm
t	time [s]
t_0	Gaussian pulse parameter
U	aid parameter in PML reflection coefficient formula
u	representative field component, solution of a generic linear equation
u_h	FEM solution
u_i	function value at a discrete point i

$\vec{u}_r$	radial unit vector
V	representative field component, voltage [V], solution space of a generic linear equation
V_h	finite-dimensional space for the FEM solution
W	aid parameter in PML reflection coefficient formula
$\tilde{W}$	aid parameter in PML reflection coefficient formula
x_n	points where values of a discontinuous permittivity function are interpolated
$x_{\pm(n+1/2)}$	collocation points of a discontinuous permittivity function
x_0	expansion point of a function
Y_i	aid parameter in PML reflection coefficient formula
Z	FDTD cell shape parameter
Z_{in}	input impedance [Ω]
$Z_{\text{in}}^{\text{cor}}$	corrected input impedance [Ω]
Z_0	characteristic impedance [Ω]
α	wave propagation direction with respect to positive x-axis [rad], wedge angle [rad]
α_i	propagation direction as a design parameter in PML optimization [rad]
Δ	FDTD cell edge length [m]
Δt	time step in FDTD [s]
Δx	x-directed cell edge length in FDTD [m]
Δy	y-directed cell edge length in FDTD [m]
Δz	z-directed cell edge length in FDTD [m]
δ	PML thickness [m]
ε	FEM solution error
$\overline{\overline{\varepsilon}}$	permittivity tensor [As/Vm]
$\varepsilon(r)$	permittivity function [As/Vm]
ε_r	relative permittivity
ε_0	permittivity of vacuum, $8.854 \cdot 10^{-12}$ As/Vm
η_0	wave impedance of free space, 376.73 Ω
θ	angle of incidence [rad]
λ	wavelength [m]
$\overline{\overline{\mu}}$	permeability tensor [Vs/Am]
μ_r	relative permeability
μ_0	permeability of vacuum, $4\pi \cdot 10^{-7}$ Vs/Am
ν	singularity exponent
π	3.14159265358…
ρ	reflection coefficient, distance from vacuum/PML interface
σ	electric conductivity [1/Ωm]
σ^H	magnetic conductivity in 1-D PML [Ω/m]
σ^N	normalized conductivity in 1-D PML
$\boldsymbol{\sigma}^N$	vector containing normalized conductivity values
σ_i^E	electric conductivity in PML [1/Ωm]
σ_i^H	magnetic conductivity in PML [Ω/m]

σ_i^N	normalized conductivity in PML
$\sigma(\rho)$	electric conductivity function in PML [1/Ωm]
σ_m	maximum conductivity on the outer boundary of PML [1/Ωm]
σ_x	electric conductivity parameter in PML [1/Ωm]
σ_x^*	magnetic conductivity parameter in PML [Ω/m]
σ_y	electric conductivity parameter in PML [1/Ωm]
σ_y^*	magnetic conductivity parameter in PML [Ω/m]
σ_z	electric conductivity parameter in PML [1/Ωm]
Φ_i	expansion function
ϕ_j	testing function
Ω	Ohm = V/A, domain
ω	angular frequency [1/s]

Abbreviations

ABC	absorbing boundary condition
CEM	computational electromagnetics
COM	complementary operators method
CPU	central processing unit
dB	decibel
DRA	dielectric resonator antenna
FDTD	finite-difference time-domain
FEM	finite element method
FFT	fast Fourier transform
HUT	Helsinki University of Technology
IEE	The Institution of Electrical Engineers
IEEE	The Institute of Electrical and Electronics Engineers, Inc.
Im	imaginary part
MB	megabyte
MoM	method of moments
ORBC	outer radiation boundary condition
PC	personal computer
PCB	printed circuit board
PEC	perfect electric conductor
PMC	perfect magnetic conductor
PML	perfectly matched layer
PSTD	pseudospectral time-domain
RCS	radar cross-section
Re	real part
RVS	resistive voltage source
SAR	specific absorption rate
TE	transverse electric
TEM	transverse electromagnetic
TLM	transmission-line matrix
UPML	uniaxial perfectly matched layer

1 Introduction

1.1 Computational electromagnetics in radio engineering

This thesis deals with the development of a selection of simulation techniques commonly applied in radio engineering. The term "computational electromagnetics" (CEM) appearing in the title of the thesis covers in the wide sense all numerical techniques applied to electromagnetic problems, and it is the most suitable general frame of reference of this work.

Concerning CEM, even if we restrict our attention specifically to radio engineering problems, there remains a multitude of computational techniques. Radio engineering is a very wide area, and it is natural that no unique method covers all applications. At least two different ways to approach and understand radio engineering concepts have developed: 1) the realm of electromagnetic fields (loosely speaking, the physicist's point of view), and 2) the realm of circuits, currents and voltages (the engineer's point of view). Both points of view *describe* reality – they are conceptual constructions that allow us, however, to design devices for practical purposes. To some extent, the choice of viewpoint is a matter of taste. However, the physical simplifications inherent in circuit theory necessarily restrict its applicability, yet making the solution of a given problem usually very efficient if applicable.

The computational techniques reflect the above-mentioned dichotomy. In this work, the point of view is mainly 1), the field point of view. Thus, in this work, we rule out numerical algorithms that are based on circuit theory. In field-based methods the circuit concepts may be used to highlight analogies to circuit theory. This is especially true for the transmission-line matrix method (TLM); circuit concepts are occasionally used also in this thesis.

Algorithms based on circuit theory simplify considerably the physics of a problem by 'coding' all relevant properties of a component (or a whole device) into a set of simple parameters, typically neglecting e.g. the physical dimensions. The dimensions of a circuit may be taken into account by connecting different parts using transmission-line models. If a circuit model is satisfactory, a circuit simulator most often provides the fastest solution. However, concerning distributed structures typical in radio engineering, such models are not necessarily easily available. It has been pointed out in the literature [2] that classical circuit design tools fail to model electromagnetic wave propagation properly along ground planes or in the empty space surrounding the circuit, and therefore a full-wave simulator could be inevitable in analyzing e.g. interference problems in printed circuit boards (PCBs).

Having adopted the field-approach, it is still possible to focus on several computational methods. Three generally used methods in radio engineering are the Finite-Difference Time-Domain method (FDTD), the Finite Element Method (FEM) and the Method of Moments (MoM). FDTD and FEM involve solution of differential equations, while MoM involves solution of integral equations. FEM can be utilized for the solution of integral equations as well, and in fact MoM could be justifiably merged to the class of finite element methods.

Radio engineering cannot be uniquely classified in terms of frequency. Practical application of the numerical techniques developed in this thesis presumes that the computational volume spans typically a few wavelengths. The corresponding frequencies depend solely on the length scales: the lowest resonance between the Earth and ionosphere is about 8 Hz - the

resonance phenomenon can be modeled using e.g. FDTD. A microdisk resonator may operate at 200 THz [3], while FDTD can again be used in the simulation. The research community's task is to find as many relevant applications as possible for a given method.

Finally, in order to be useful for a radio engineer, a numerical method must be able to model material properties in the relevant frequency range, and at least a power source, sometimes also lumped elements. There are significant differences between the suitability of FDTD, FEM and MoM to different types of problems. Examples highlighting typical use of each method could be radiation absorption in biological tissue for FDTD, resonance mode analysis for FEM, and scattering from a perfectly conducting body for MoM. Generally, it seems that FEM has lost some of its popularity in favor of FDTD in high-frequency electromagnetics. Instead, MoM continues to be popular, especially in antenna engineering. Nevertheless, MoM is not considered further in this thesis.

For the algorithms to be discussed in this work, we made the presumption of "a few wavelengths" regarding the size of the computational domain. Towards lower frequencies (sub-λ scales), the use of (non-radiating) circuit models is better justified. In low-frequency problems not conveniently expressible as equivalent circuits (e.g. magnetic field in electric motors), the field problem is usually reformulated as a quasi-static approximation. For such problems, FEM is a suitable tool, rather than FDTD. Towards higher frequencies (details many hundreds of wavelengths), we are entering into the realm of optics, where a statistical collection of 'rays' can properly represent the operation of a system under consideration. The popular ray-tracing method [4] used to analyze e.g. mobile phone reception is an example of such quasi-optical methods applied in radio engineering. The highest electromagnetic frequencies known belong to the realm of nuclear physics, where the particle-like nature of photons is determinative, and classical field theory may not be appropriate.

Some computational methods are more specialized for solving purely radio engineering problems, some others can easily be exploited by the analogies between physically unrelated phenomena. A common factor of the techniques of this thesis, however, is always a wave.

1.2 Objectives of this study

Even though numerical methods have been applied for tens of years in electrical engineering, development work continues with increasing intensity worldwide. The diversity of applications of electromagnetic phenomena has been the source of more and more specialized numerical techniques. In this thesis, an attempt is made to develop computational techniques in such a manner that as much generality as possible is maintained, so that the proposed developments could be applied to a wide variety of problems. Furthermore, to demonstrate a typical numerical modeling process, a sample problem is discussed in [P3] and chapter 4 that serves other research project carried out at the Radio Laboratory.

1.3 General remarks about modeling and numerical methods

The mathematical form of physical laws makes it possible to efficiently apply numerical methods to describe real world phenomena. The fact that mathematics has proven to be a reliable guide to our way of describing the physical world has literally revolutionized our worldview and everyday life from the days of Galileo Galilei, one of the first scientists who

clearly understood that “the laws of nature have been written with mathematical letters”. Nowadays, we are so used to technology that we seldom pay attention to the philosophical principles beyond it. Once electricity was invented and industrialized, it soon became an apparent triviality: “electricity comes from a wall socket.”

A computer understands only plain numbers, not physical quantities. Usually an engineer wants to interpret computed numbers in physical units. From the computer’s point of view, this is done only for convenience, even though it may sometimes be misleading. One may get the false impression that a computer program really “understands” the distinction between e.g. small-scale and large-scale models, while in fact the program and the processed numbers may be identical in both cases. Most materials show nonlinear behavior in extreme conditions, but one must not think that this behavior is seen in a model just by making dimensions smaller or intensities higher, if the nonlinear behavior is not specifically implemented in the code. Everyone who applies numerical methods should be aware of the assumptions and restrictions covering the algorithms.

To simplify terminology, let us define “numerician” as a person whose main task is to apply methods of numerical analysis in engineering or scientific problems. He or she is found somewhere between mathematicians, physicists and engineers. He or she is responsible for expressing an engineering problem in physical terms, choosing or developing a numerical method for the solution, writing and/or executing a code, and finally interpreting and explaining the results. As complicated numerical modeling has, in many cases, become part of the engineering design cycle, the number of numericians is large, even though they are usually not called by that title.

Radio engineering, in particular, provides very interesting challenges for a numerician. From the mathematical point of view, adopting the field-approach, many radio engineering problems can be reduced to the problem of finding solutions to Maxwell’s equations in different geometries, with different sources and different materials. Even though it may seem to be a unified and a rather simple task, in fact it is not. Attempts have been made to unify the modeling through commercial general-purpose computer programs, though with considerable success. However, novel techniques providing improvements for a limited class of problems are continually proposed by the modelers worldwide.

Numerical modeling in radio engineering has nevertheless matured to a highly useful level. Quantities that can be extracted from a simulation are e.g. *S*-parameters, impedance of an antenna or a microstrip line, radiation pattern, specific absorption rate values (SAR), mutual impedance of antennas, resonant frequencies, current distribution, radar cross-section (RCS), or virtually any quantity of interest. The difficult question is “What is the accuracy of the computed results?” Fortunately, on our path to answering this question, there are problems to which the exact solutions are known. Comparing computed results with the reference solutions gives us an idea of the accuracy of the applied method. We are not ‘blind’ while testing an algorithm; where standard algorithms are concerned, we know at least the asymptotic behavior of the error. The problem is that the error formulae often contain unknown coefficients, and the asymptotic behavior may not be seen with given resources. Therefore, reference problems are very important ‘lighthouses’: to obtain a higher level of reliability, a method should always be tested with a set of problems having known solutions. In practice, an exact mathematical solution is only available for the simplest problems, and quite often one has to rely on ‘best available’ reference solution, which is usually either a measurement or another computed solution.

Being able to give absolute bounds to an error in a nontrivial problem is a very happy incident. Let us mention two examples. An inherent property of the FDTD method (to be discussed later) is that a wave in the numerical model always propagates in a velocity *less* than the physical velocity. This leads to a systematic shift of frequency domain results towards lower frequencies. Therefore, while evaluating the resonant frequencies of a resonator, the exact values will be approximated *from below*. Instead, using FEM, one can show that the eigenvalues corresponding to resonant frequencies are always approximated *from above*. Thus, the true solution is sandwiched between these two. The other example is reported in [5-7], where the impedance of a transmission line is evaluated using FEM for the solution of original and dual problems. Again, one of the formulations leads to approximation *from below*, while the other leads to approximation *from above*.

Among the important contributions of numerical methods is that they can make the invisible visible: nobody has ever seen a radio wave, but a simulation can make it possible. Visualization is a very efficient tool in building intuitive concepts. The development of computer technology has made the visualization generally feasible. There is also a possible danger here: a user might be impressed by colorful pictures or movies even though they might not make any sense. A quick look at a selection of related advertisements reveals that visualization is indeed used as a marketing trick. A user must not be confused with the fact that numerical modeling is one thing, and representation of the results through visualization is another thing, secondary to the first.

The common ‘headaches’ met by every numerician are the following:

- What is the physical model? Usually a practical problem is too complicated to be modeled completely, with every factor not even known beforehand. One has to decide what the essential characteristics of a given problem are.
- Having chosen the physical model, one has to choose a relevant numerical method. Due to inherent restrictions of the methods, one may have to compromise e.g. by inaccurate description of the geometry of the physical model (staircasing errors etc.). From the mathematical point of view, application of a numerical algorithm always introduces some error such that the computed values only approximate the compromised physical model that approximates the already idealized physical model. Only in exceptional cases can one undoubtedly bound the error due to the discretization of the continuous model.
- Finally, based on simulations and experience, a real prototype is fabricated. The prototype only approximates the intended physical model; in the fabrication process some unknown uncertainty is always introduced.
- The measurement conditions of the prototype may differ from the real operating conditions, due to measurement cables, weather, noise or other similar reasons.

In short, a numerical model approximates a compromised physical model that approximates an actual physical model that is approximated by the prototype that approximates the final product. A numerician has to live with approximations.

1.4 Contents of the thesis

In this thesis, two numerical methods are discussed that are widely used in radio engineering, namely FDTD and FEM. FDTD covers roughly 80 % of the work, and FEM about 20 %.

Reflecting this, there are three chapters devoted to FDTD and one to FEM. In these chapters, the basics of the methods are briefly reviewed and references are given to literature. The algorithm developments reported in papers [P1-P6] are explained, leaving most of the technical details to the papers themselves. In the summary of the publications, each paper is briefly introduced and commented on. Finally, in the conclusions chapter, the main contribution of this work is collected, along with some proposals for future work.

The area of computational radio engineering is enormous, and it is impossible to include a reference to all relevant topics treated in the literature. It is demonstrative that a recent survey done by K. L. Schlager and J. B. Schneider of only FDTD literature [8] contained 496 references plus 68 references to novel application areas of FDTD. The growth in the number of publications has been almost exponential during the 90's. In the year 1996 alone, there were at least 430 publications related to FDTD, and the rate must have grown further since then. Schlager and Schneider had a cumulative catalogue of over 2300 FDTD-related publications as of December 1997. A search in IEEE/IEE Electronic Library using search terms "FDTD" or "FD-TD" yielded 1973 hits in October 2000 – the database contains publications only from 1988 onwards. In this thesis, the literature is reviewed to an extent suitable for constituting a background for the original work presented. It is possible to write a working FDTD code based on the details given either in this thesis or in the references.

Concerning FEM and MoM, the number of related publications is also enormous. A similar search in the IEEE/IEE Electronic Library yielded 1635 hits for "FEM" and 592 hits for "MoM". Already in the year 1977, Zienkiewicz mentioned the existence of close to 8000 FEM-related references [9]. Selected references relevant to this work are given.

The second part of this thesis contains the papers included. The scientific contribution of the thesis is reported in detail in these papers.

2 Finite-Difference Time-Domain method

The finite-difference time-domain method is a powerful yet a simple algorithm to solve Maxwell's equations in time-domain. FDTD was introduced first time by Yee in 1966 [10]. At that time computers had very limited capabilities in terms of core memory and CPU speed. Furthermore, the number of computers was low, and computing time was luxury. This may be the reason why FDTD did not get much attention for years; FDTD makes sense only if sufficient computer resources are available. As it turned out, developing FDTD to a useful level required significant effort from a large number of researchers worldwide.

Things started to change in 1975, when Taflove and Brodwin published their highlight paper [11]. There are several merits of [11]: a) it recognizes the potential of FDTD to solve complicated electromagnetic problems and wakes up interest towards FDTD; b) a working absorbing boundary condition (ABC) is presented; c) a "modern" way to implement transparent plane wave source is given; d) the stability criterion is correctly derived; e) exploitation of problem symmetry is discussed. Since FDTD is treated in [11] more or less as a competitor to traditional frequency-domain methods, the examples given involve only sinusoidal excitation.

The first applications of FDTD were scattering and penetration problems. As increasing number of researchers devoted themselves to the development of FDTD, more and more applications of the method were found.

2.1 Standard FDTD algorithm

2.1.1 Discretization of Maxwell's equations

The starting point of the FDTD algorithm is the differential form of Faraday's and Ampere's laws, or Maxwell's curl equations:

$$\nabla \times \vec{E} = -\partial_t \vec{B}, \tag{1}$$

$$\nabla \times \vec{H} = \vec{J} + \partial_t \vec{D}, \tag{2}$$

where, as usual, $\vec{E}$ and $\vec{H}$ denote the electric and magnetic field intensities, respectively, $\vec{D}$ and $\vec{B}$ denote electric and magnetic flux densities, respectively, and $\vec{J}$ denotes electric current density. In a basic discussion, we can assume linear constitutive relations,

$$\vec{B} = \mu_0 \mu_r \vec{H}, \qquad \vec{D} = \varepsilon_0 \varepsilon_r \vec{E}, \tag{3}$$

where μ_0 and ε_0 are the permeability and permittivity of vacuum, respectively, and the dimensionless quantities μ_r and ε_r are the relative permeability and permittivity of the medium, respectively. For the moment, we assume that μ_r and ε_r are scalar functions of position, representing isotropic, possibly inhomogeneous, medium.

The philosophy behind FDTD is to interpret (1) and (2) as a way to 'update' the field quantities appearing in the time derivatives. For example, Equation (1) can be read as "the

time rate of change of $\vec{B}$ is equal to the negative of the curl of $\vec{E}$". Hence, if we know the curl of $\vec{E}$, we can compute an infinitesimal change of $\vec{B}$:

$$d\vec{B} = -dt(\nabla \times \vec{E}). \tag{4}$$

If, furthermore, some initial value of $\vec{B}$ and a finite time step Δt are chosen, we can perform a single update step to $\vec{B}$:

$$\vec{B}_{new} = \vec{B}_{old} - \Delta t(\nabla \times \vec{E}). \tag{5}$$

In practice, the number of vector fields is reduced to two by the constitutive relations (3). Quite often $\vec{E}$ and $\vec{H}$ are chosen as working variables.

In FDTD, an advantageous discretization of field quantities is chosen [10], resulting local approximations of second-order with respect to the grid parameters. The spatial arrangement of field components in the so-called Yee grid is depicted in Figure 1. Note that in a large grid, there are six field component locations per unit cell. The $\vec{E}$- and $\vec{H}$- fields are defined at time levels offset by $\Delta t/2$. The following notation is used for any field component F, when evaluated at a discrete point at a discrete time:

$$F(i\Delta x,\, j\Delta y, k\Delta z, n\Delta t) = F^{n}_{i,j,k} \tag{6}$$

where Δx, Δy and Δz are the spatial increments of the grid, here assumed uniform throughout the grid. Using this notation and Yee's discretization, we can write the update step for H_x:

$$\begin{aligned} H_x\big|^{n+1/2}_{i,j+1/2,k+1/2} &= H_x\big|^{n-1/2}_{i,j+1/2,k+1/2} + \Delta t/(\mu_0\mu_r(i,\, j+½, k+½))\times \\ &\left[\left(E_y\big|^{n}_{i,j+1/2,k+1} - E_y\big|^{n}_{i,j+1/2,k}\right)/\Delta z - \left(E_z\big|^{n}_{i,j+1,k+1/2} - E_z\big|^{n}_{i,j,k+1/2}\right)/\Delta y\right]. \end{aligned} \tag{7}$$

Other components are updated similarly. Electric field update equations are slightly modified, if the medium has finite conductivity σ, giving rise to volumetric current density $\vec{J}$. Assuming an ohmic relationship between electric field intensity and current density, we can write the Ampere's law in the form

$$\varepsilon_0\varepsilon_r\partial_t\vec{E} + \sigma\vec{E} = \nabla \times \vec{H}. \tag{8}$$

In the discretization of (8), a quasi-implicit interpolation in the conductivity term is used:

$$\sigma\vec{E}^{\,n+1/2}_{i,j,k} = \sigma\left(\vec{E}^{\,n}_{i,j,k} + \vec{E}^{\,n+1}_{i,j,k}\right)/2. \tag{9}$$

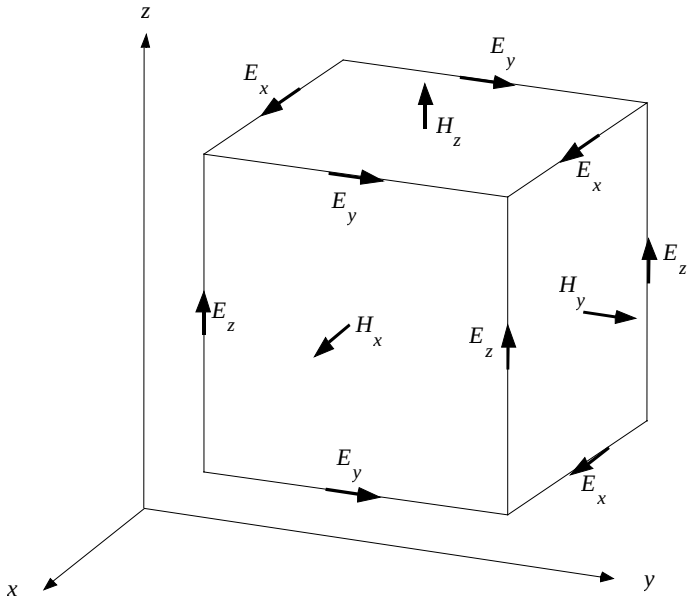

Figure 1. Yee's unit cell.

The resulting equation is easily turned into an explicit time step. As an example, let us write the update step of E_x:

$$
\begin{aligned}
&a(i,j,k) := \sigma(i,j,k)\Delta t/(2\varepsilon_0\varepsilon_r(i,j,k));\\
&E_x\Big|_{i+1/2,j,k}^{n+1} = \frac{1-a(i+\tfrac{1}{2},j,k)}{1+a(i+\tfrac{1}{2},j,k)}E_x\Big|_{i+1/2,j,k}^{n} + \frac{\Delta t}{\varepsilon_0\varepsilon_r(i+\tfrac{1}{2},j,k)\left(1+a(i+\tfrac{1}{2},j,k)\right)}\times \qquad (10)\\
&\left[\left(H_z\Big|_{i+1/2,j+1/2,k}^{n+1/2} - H_z\Big|_{i+1/2,j-1/2,k}^{n+1/2}\right)/\Delta y - \left(H_y\Big|_{i+1/2,j,k+1/2}^{n+1/2} - H_y\Big|_{i+1/2,j,k-1/2}^{n+1/2}\right)/\Delta z\right].
\end{aligned}
$$

While writing (7) and (10), we have emphasized that the material parameters ε_r, μ_r and σ are allowed to be functions of position, yet not complicating the modeling of inhomogeneous problems. Running an FDTD program is essentially nothing but repeatedly updating the field values according to Equations (7) and (10) (and similar update steps for the other components), and recording desired field quantities during the simulation.

Even though the update equations involve only the time-dependent Maxwell's equations, the discretized divergence equations will be automatically satisfied, that is, the FDTD algorithm introduces no artificial sources [12].

2.1.2 Spatial grid, time step and computational burden

While defining an FDTD model for a given problem, one has to choose proper grid parameters. There are two rules that restrict this choice: (i) the spatial increment must be small enough to resolve the shortest wavelength well enough. A rule-of-thumb is that the shortest wavelength must correspond to at least five unit cell diagonals. (ii) Any geometrical detail must be represented well enough by FDTD cells. Another rule-of-thumb is that the

smallest geometrical dimension should be divided into at least two or three cells. The final choice of the grid parameter is the more restrictive of these two.

Once spatial increments are chosen, the time step is bounded from above via a stability condition [11]:

$$\Delta t \leq \left(c\sqrt{1/\Delta x^2 + 1/\Delta y^2 + 1/\Delta z^2} \right)^{-1}, \qquad (11)$$

where c is the highest wave propagation velocity in the problem, usually the speed of light in vacuum. Since a shorter time step does *not* improve the accuracy, one usually chooses a value for Δt that is close to the stability limit. The corresponding coefficient is frequently called the Courant-number.

After definition of grid parameters, one can estimate the computational burden [13]. For an inhomogeneous problem with finite conductivity, there are six real variables (field variables) and nine 1-byte integers (material parameter indexes) to be stored for each cell. A typical problem comfortably solvable by a present day PC spans, say, 100×100×100 = 1.000.000 cells. If one uses double-precision arithmetic (8 bytes/word), such a problem requires about (6×8B + 9×1B) ×1M = 57 MB of memory. There is certain overhead due to a number of auxiliary variables, but one easily gets an idea of the order of the resources needed.

2.1.3 Excitation

Special attention has to be paid to the excitation of the FDTD simulation. Application of update equations makes sense only if either some initial conditions are given, or if energy source is applied. Since nontrivial initial conditions cannot usually be specified, the system is most often excited by a source.

There are many case-dependent source models available. The simplest one is the so-called hard source: some field components at some locations are given pre-defined values in time-domain, while the other field values are updated normally. The problem of the hard source is that any reflected wave returning back to the source will be perfectly re-reflected – hence the name.

To make the source transparent for the reflected waves, the system can be excited using an additive source term [11]. Since the source is totally separated from the field interactions, it can be placed inside a structure yet not forming part of it [14].

Exciting a single electric field component at one location represents a Hertz dipole. To simulate a magnetic dipole, one can correspondingly excite a single magnetic field component. Such point sources are sometimes useful in theoretical considerations, but most practical problems involve more complicated source fields. One frequently used source model is a plane wave source, already used in the very first applications [11]. In the simplest case, one can produce a plane wave by choosing field locations along a line parallel to some of the coordinate directions, and applying the added source technique. This can be generalized easily to diagonal directions also. A plane wave propagating in arbitrary direction can conveniently be realized as follows: one can separate the incident and scattered fields (in linear media), and use FDTD equations only to the scattered field, provided the incident field

is known analytically [13]. This is especially useful in pure scattering problems, like radar cross-section (RCS) calculations.

Considering transmission lines, to excite a certain propagation mode, one must first find out the transverse field distribution, at least approximately. For many simple transmission line structures, like a microstrip line enclosed in a waveguide, the excitation can be done as follows: a 2-D FDTD is used to find the cut-off frequencies of the modes of interest [15-17]. Next, the simulation is repeated with a uniform excitation profile, and a Fourier-transform is performed at the cut-off frequencies for all field locations. The field profile is then extracted from the Fourier transforms [O7]. A simplified method is to excite an approximate transverse field, and let the wave propagate some distance along the line before reaching the actual scattering structure. There are cases supporting the conception that a quite rough approximation of the field profile suffices, and the source can therefore put very close to the scatterer [14].

Another important excitation case is the modeling of a coupling probe formed from an extension of the inner conductor of a coaxial cable. This type of feed is common in antennas. There are several modeling options, of which two common are: a) modeling the source as an equivalent delta-gap [18], and b) modeling the coaxial cable as a separate 1-D structure and connecting it to the FDTD volume using a special technique [19,P3]. Closely related to a), the so-called resistive voltage source simulates also the feed port impedance, being otherwise similar to the delta-gap [2,20,21]. The feed models are discussed further in Chapter 4.

Since FDTD is a time-domain method, one usually specifies the time variation of the excitation as a Gaussian pulse containing a wide frequency band. If preferred, sinusoidal excitation may also be used. Once the time step Δt, center frequency f_0 and bandwidth of the pulse f_w are chosen, a proper temporal discretized waveform $u(n)$ of the excitation is

$$\begin{aligned} T &= 1/(f_w \Delta t), \\ t_0 &= 5T, \\ u(n) &= \exp\left(-((n-t_0)/T)^2\right)\sin\left(2\pi f_0 n \Delta t\right). \end{aligned} \tag{12}$$

2.1.4 Boundary conditions

Some boundary conditions must be applied on the outer boundary of the FDTD volume. In most cases it is one of the following: (i) perfect electric conductor (PEC) or electric wall, $\rho = -1$; (ii) perfect magnetic conductor (PMC) or magnetic wall, $\rho = +1$; (iii) absorbing boundary condition (ABC), $\rho = 0$. PEC is used to represent ideal conductors; PMC may be applied on symmetry planes to reduce the size of the computational volume. ABC is used to absorb outgoing waves, and it is sometimes called outer radiation boundary condition (ORBC).

The most challenging boundary condition is ABC. It is needed to simulate an infinite open space, to prevent outward going waves reflecting back to the solution region. Usually one cannot choose the simulation volume so large as to causally isolate reflections from the outer boundary from the solution region. There is a multitude of ABC's for FDTD algorithm available. Two common ABCs are the Mur absorbing boundaries [22] and Berenger's Perfectly Matched Layer (PML) [23]. In short, Mur ABC is extremely simple to implement

while still providing satisfactory absorption for a great variety of problems. Berenger's PML requires considerable enlargement of the computational volume, but is essentially frequency-independent, superior to most ABCs and rather easy to implement, too. Most often, if computer memory and ease of programming is determinative, one uses Mur ABC; otherwise the choice is PML. ABCs are discussed in more detail in Chapter 3.

Many structures are only partially open; the structure may contain an infinite ground plane, it may be enclosed inside waveguide walls, it may have a plane of symmetry where PMC is applicable etc. In these cases ABC has to be implemented in only some of the bounding surfaces. This may make for example PML a much less expensive choice. For instance, consider a structure spanning 100×40×20 = 80.000 cells. A typical PML requires extension of the volume by 10 cells on each boundary. If the problem is totally open, a PML implementation requires 120×60×40 = 288.000 cells = 3.6×size of the original problem. If, instead, the structure is enclosed in a waveguide such that only the ends in the longitudinal direction are open, the PML implementation would require only 120×40×20 = 96.000 cells = 1.2×size of the original problem.

In FDTD terminology, "boundary conditions" means usually the *outer* boundary conditions. Of course, material interfaces are also boundaries, and some boundary conditions have to be applied to connect each side of the interface. These conditions can be implemented in a very simple manner. Referring to Figure 1, it is advisable to arrange the FDTD lattice such that the electric field components are tangential to the interfaces. Since the physical boundary condition requires continuity of the tangential electric field, this requirement is automatically satisfied by this arrangement. To update the tangential electric field components at the interface, one has to average the relative permittivities on each side [24].

2.2 On the accuracy of the FDTD algorithm

2.2.1 Second-order accurate differences

The arrangement of field components in Yee cell (Figure 1) allows using central differences in the discretization of the spatial derivatives in the Maxwell's equations. Also, the electric and magnetic field components are interleaved by half a time step, in order to apply central differences in the time derivatives.

A basic analysis of the accuracy of the finite differences is based on Taylor expansions of the field quantities. Suppose u is a representative field component. We have the following expansions:

$$u(x_0 \pm \Delta x/2) = u(x_0) \pm (\Delta x/2)u'(x_0) + (\Delta x^2/8)u''(x_0) \pm (\Delta x^3/48)u'''(x_0) + O(\Delta x^4). \quad (13)$$

Subtracting and dividing by Δx:

$$\big(u(x_0 + \Delta x/2) - u(x_0 - \Delta x/2)\big)/\Delta x = u'(x_0) + (\Delta x^2/24)u'''(x_0) + O(\Delta x^3). \quad (14)$$

Following the notation (6), we thus write the approximation to the derivative at point i:

$$(D_h u)_i = (u_{i+1/2} - u_{i-1/2})/\Delta x. \quad (15)$$

From the remainder term in (14), we see that the local error of the approximation (15) is proportional to Δx^2. Accordingly, the local error in the approximation of the time derivative is proportional to Δt^2. It follows from the Lax-Richtmyer equivalence theorem that if the algorithm is stable (that is ensured by the stability condition (11)), then the difference between the exact and numerical solutions is of the order $O(\Delta x^2)+O(\Delta t^2)$ in a suitable norm *at all time steps* [8, p. 64]. Hence, FDTD is called a second-order algorithm. Note that this statement is based on the assumption of proper smoothness of the solution.

2.2.2 Numerical dispersion

For a fixed cell size, different frequency components of a wave propagate at slightly different velocities. This phenomenon is called numerical dispersion, and it is inherently present in the FDTD algorithm. Furthermore, velocity depends also on the angle of propagation with respect to the coordinate axis. The latter is sometimes called numerical anisotropy, but usually these two effects are combined in the single term "numerical dispersion". Incidentally, waves propagate in the numerical grid always at a velocity *less* than the physical velocity.

The basic effect of numerical dispersion is that it produces a cumulative phase error that is in general difficult to predict, even though bounds can be calculated. In sinusoidally excited simulations, the phase error may distort the results significantly, e.g. if the operation is based on phase cancellation. In wide-band simulations, numerical dispersion appears as a shift of frequency domain results towards lower frequencies.

The analysis of numerical dispersion is rather easy, and is based on application of FDTD equations to a representative plane wave. The dispersion is best expressed as the numerical dispersion relation [P1]:

$$\left(\sin\left(\omega\Delta t/2\right)/(c_0\Delta t)\right)^2 = \left(\sin(k_x\Delta x/2)/\Delta x\right)^2 + \left(\sin(k_y\Delta y/2)/\Delta y\right)^2 + \left(\sin(k_z\Delta z/2)/\Delta z\right)^2 \quad (16)$$

where (k_x, k_y, k_z) is the numerical wave vector. Equation (16) can be solved for numerical wave vector using Newton iteration.

From (16) we see that numerical dispersion relation approaches quadratically the physical one, as the grid parameters are decreased, manifesting the second-order nature of the algorithm. In order to keep the numerical dispersion small, one has to choose small enough grid parameters, with respect to smallest wavelength considered. For cubical cells, resolution $\lambda = 10\Delta x$ assures that the maximum dispersion error is less than 1.15 %. Resolution $\lambda = 20\Delta x$ reduces the maximum error to 0.28 %. For non-cubical cells the dispersion is more severe.

Section 2.4 deals with a dispersion error cancellation procedure developed in [P1].

2.2.3 Errors in quantities obtained via FFT

The frequency-domain information is efficiently obtained from an FDTD simulation via the application of fast Fourier transform (FFT) to the time-domain response. A few points need special attention, while interpreting the frequency-domain results. The most important is the

effect of truncating a signal; FDTD simulations involve a finite number of time steps, and in practice the simulation is truncated after a suitable criterion is met. Such criterion may be for example sufficient dissipation of energy via losses or radiation. In practice, the monitored signal is never completely died off. Truncation of a non-zero signal corresponds to high-frequency noise that may be aliased to the desired band. An estimation of this noise is given by the ratio of truncated amplitude to the maximum amplitude of the signal.

Basically the same applies, if one improves the resolution in frequency-domain via so-called zero-padding, i.e. artificial lengthening of the signal by a suitable number of zeros, usually to make the signal length equal to some power of two. Ideally, if a signal has compact support in time-domain, i.e. if it is exactly zero after a finite number of time steps, zero-padding does not introduce any error, but if the signal is suddenly switched off, truncation noise will occur. Therefore, zero-padding can only be used for sufficiently damped responses.

As a final point, the dynamic range of the computer arithmetic plays sometimes a crucial role, especially if single-precision arithmetic is used. Consider the following fictitious example: only the fundamental mode is to be excited in a waveguide containing discontinuities. The discontinuities excite higher-order modes. We do not want these higher modes to propagate down the guide. The spectral components of the excitation at and close to the cut-off of the fundamental mode will remain ringing, causing truncation noise. Therefore, the excitation must be designed such that the spectral components are low enough at first cut-off, say –100 dB below maximum. Also, the propagation of higher modes will be suppressed by designing the spectral components low enough at the cut-off of the 2^{nd} mode, say –100 dB again. Since the dynamic range of single-precision arithmetic is about 140 dB, we have only about 40 dB dynamic range in our simulation at frequencies close to the cut-offs.

2.2.4 Cases where accuracy is reduced

The accuracy of FDTD is not always of second order. Optimal convergence assumes certain smoothness, namely that third derivative of the solution is bounded. This requirement is not met, for example, on the interface between two dielectrics; in this case, however, if the material parameters are averaged on the boundary [24], overall second-order accuracy is recovered.

Field singularities also reduce the smoothness of the solution. Consider a fin line [25] depicted and schematically discretized in Figure 2. Close to the tips of the fins, the transverse fields are singular and behave as $1/r^{1/2}$. Simulation tests with the structure reveal that the convergence rate is clearly reduced to first order. Figure 3 shows the relative error of the cut-off frequency of the lowest TE-mode as a function of grid parameter. The reference result is obtained using FEM equipped with singular basis functions [P6].

Sometimes the error related to staircasing of a smooth structure results in reduction of convergence rate. In [26], Harms *et al.* study the resonant frequencies of a circular cavity using both conventional FDTD and a nonorthogonal modification. They find that staircasing reduces the order of convergence of resonant frequency to approximately $h^{1.5}$, where h represents the cell size. Turkel reports in [8, Chapter 2] results related to circular annular region, and the staircasing is seen to yield first-order convergence in L_2-norm. Note, however, that the error measure is different in these cases.

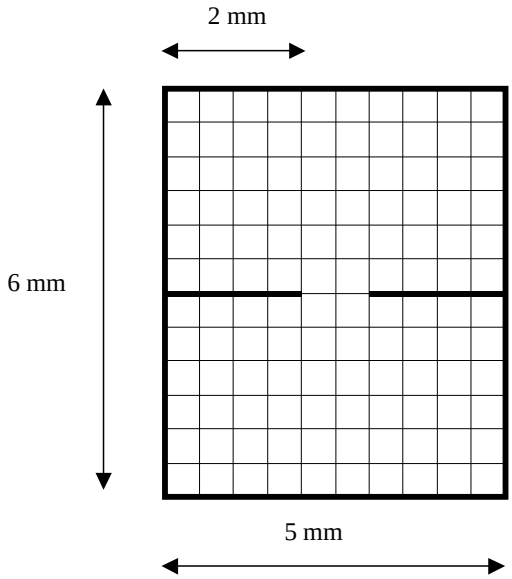

Figure 2. Crosscut of a fin line supporting transverse field singularities.

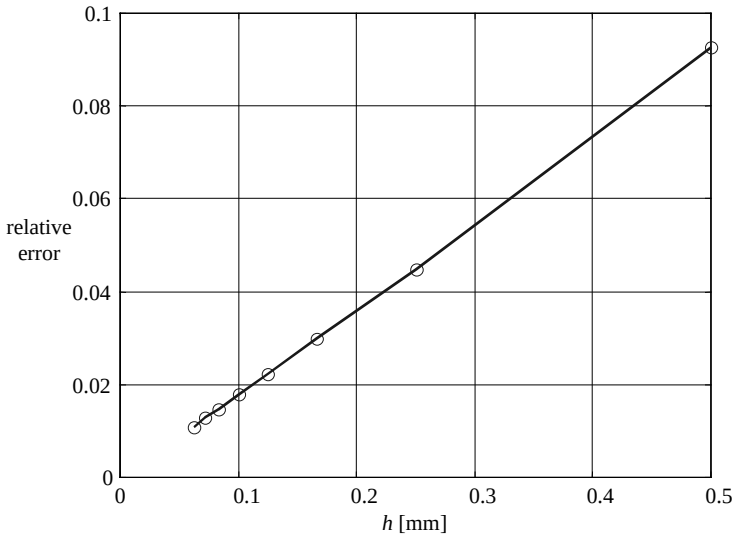

Figure 3. Relative error of the lowest cut-off frequency of the fin line shown in Figure 2 as a function of grid parameter.

A 'pathological' combination is a circular fin line, where both staircasing and field singularity are present. The exact cut-off frequencies are analytically known, and Figure 4 presents the relative error as a function of grid parameter. For comparison, the corresponding error of an empty circular waveguide is also plotted. We see that the convergence rate is again essentially linear. The nonmonotonic convergence for large values of h is due to coarseness in the approximation of the geometry of the circular disk.

Linear convergence limits severely the obtainable accuracy: in 2-D problems, computational burden is proportional to $1/h^3$, and linear convergence implies that gaining one order of magnitude in the accuracy would require 1.000-fold work, to be compared with the usual 32-fold work of second-order convergence. The corresponding numbers in 3-D problems are 10.000 versus 100. To restore second-order convergence, there is a wide selection of variations of FDTD that take into account curved boundaries [27]. A good review is presented in [28]. Modifications for the field singularity problem are found in e.g. [25,29].

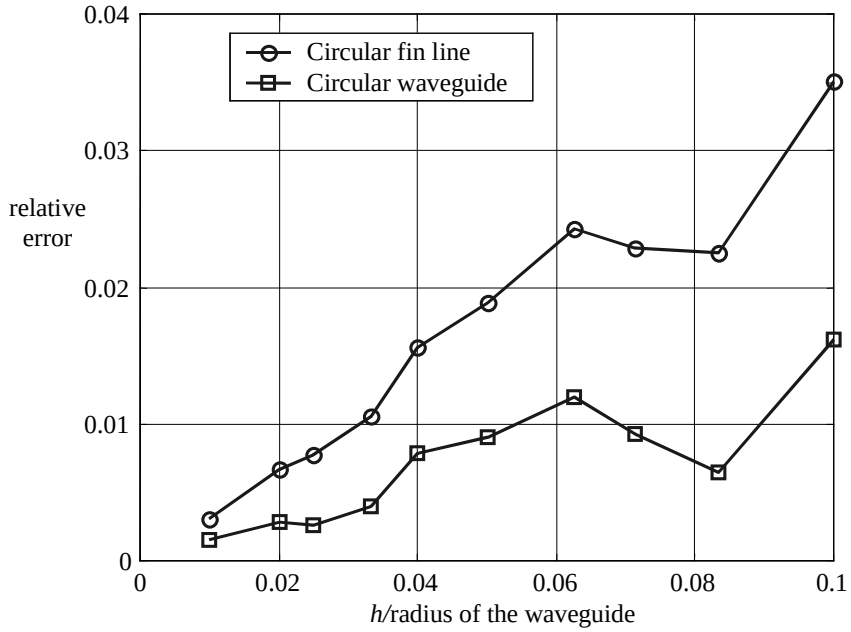

Figure 4. Relative error of the lowest cut-off frequency of a circular fin line and a circular waveguide as a function of grid parameter.

2.3 High-order methods

There are schemes where the local truncation error is higher than second order with respect to grid parameters, thus expecting better accuracy. A good review of high-order methods is given by Turkel in [8, Chapter 2]. High-order finite differences belong to classical numerical analysis, but their use in the solution of electromagnetic problems is a rather new subject. Of the early works that are clearly FDTD-type let us mention [30] and [31]. Here, we review high-order algorithms briefly and discuss the possible advantages over standard FDTD.

2.3.1 Fourth-order accurate spatial derivatives

Due to large number of field variables and time steps involved, any 3-D time-domain algorithm must be essentially explicit. One cannot afford inversion of a very large system of equations during each time step, apart from tridiagonal systems, whose inversion requires only a linear amount of operations. A tridiagonal compact implicit scheme has been introduced by Turkel and Yefet [32], and independently by Young *et al.* [33]. In this scheme, the approximations of spatial derivatives are obtained through a fourth-order accurate implicit equation compatible with the Yee's stencil:

$$\frac{1}{24}\left(\left(D_h u\right)_{i+1} + \left(D_h u\right)_{i-1}\right) + \frac{11}{12}\left(D_h u\right)_i = \left(u_{i+1/2} - u_{i-1/2}\right)/\Delta x. \qquad (17)$$

Solution of (17) for $\left(D_h u\right)_i, i = 1,2,...,n$ involves a tridiagonal system of equations per grid line, so the workload is acceptable. The spatial derivative operator defined by (17) is called

Ty-operator of order four. If the associated time stepping scheme is of order *p*, then the corresponding FDTD algorithm is called *Ty*(*p*,4).

2.3.2 Derivatives on the outer boundary

Even though scheme (17) uses exactly the same finite differences than standard FDTD, outer boundary treatment requires special attention, because system (17) must be closed. For that, Turkel proposes an implicit fourth-order one-sided approximation of the derivatives on the boundaries [32]:

$$\left(26\left(D_h u\right)_{1/2} - 5\left(D_h u\right)_{3/2} + 4\left(D_h u\right)_{5/2} - \left(D_h u\right)_{7/2}\right)/24 = (u_1 - u_0)/\Delta x. \qquad (18)$$

The resulting closed system of equations can easily be manipulated back to tridiagonal form.

Gustafsson has proved [34] that the overall accuracy is not reduced, if the approximation scheme is *one* order less accurate on the boundary, as compared to the inner domain. However, if one applies the simple second-order accurate FDTD approximation to the derivative on the boundaries, then the global accuracy is reduced to third order. Concluding, use of (18) is recommended.

2.3.3 Time stepping

To approximate the temporal derivatives in the Maxwell's equations, one can choose either the standard second-order leapfrog time stepping scheme (*Ty*(2,4)-algorithm) or some fourth-order scheme (*Ty*(4,4)-algorithm). The fourth-order time stepping schemes are realized either using the classical Runge-Kutta integration, or using the Maxwell's equations themselves to convert time derivatives into space derivatives.

Generally, in a numerical algorithm, the error sources should be well balanced. In fourth-order FDTD algorithms the error is proportional to $O(\Delta t^p)+O(\Delta x^4)$, where p is the time stepping order. We see that in a (2,4)-algorithm we have a control over the time discretization error simply through the time step. Contrary to the Yee's algorithm, the optimal choice of the time step is much less than required by the stability criterion. In *Ty*(2,4) the optimal time step in 2-D is seen to be about $\Delta t = \Delta x/(18c_0)$ [32]. For *Ty*(4,4) the optimal time step is about $\Delta t = \Delta x/(4c_0)$. It turns out that the resulting accuracy of *Ty*(2,4) and *Ty*(4,4)-algorithms is comparable. The workload is about the same, because *Ty*(4,4) involves four-stage Runge-Kutta integration, and therefore the effective optimal time step in *Ty*(4,4) is $\Delta t = \Delta x/(16c_0)$.

Since more storage and complexity is needed to implement the *Ty*(4,4)-algorithm without any essential improvement over the simpler *Ty*(2,4)-algorithm, the latter is highly preferred. Furthermore, it is more compatible to the existing FDTD codes. These reasons have resulted in relative success of (2,4)-algorithms in the research community.

A peculiar observation is that the energy fluctuations in Yee's FDTD are much smaller than in *Ty*(2,4)-algorithm. Reducing the time step reduces the fluctuations in Yee's FDTD but not in *Ty*(2,4). This phenomenon is anticipated being related to unequal orders of convergence with respect to space and time.

2.3.4 Material interfaces

Discontinuous material parameters are an essential feature of most of the practical simulation problems met in radio engineering. Material interfaces reduce the smoothness of the field quantities.

In fourth-order algorithms, there are at least two ways of treating material interfaces, [8, Chapter 2] and [35]. In [8], related to *Ty*(*p*,4)-algorithms, the discontinuous $\varepsilon(r)$ is replaced by a smooth implicit interpolation of $\varepsilon(r)$. This results in change of the whole $\varepsilon(r)$, not only at discontinuities. However, the change is very small far from the discontinuity, see Figure 5.

In [35], the algorithm involves wider stencils than *Ty*(2,4), and the field values next to the material interface are manipulated at each time step to enforce proper smoothness to the solution. Both [8] and [35] report improved accuracy of the results compared to simple arithmetical averaging of the material parameters. In [8] it is justified that the implicit interpolation preserves the basic fourth-order accuracy of the *Ty*-algorithm, at least in the cases studied.

In other words, even though the physical field quantities have reduced order smoothness, it is advantageous to enforce additional non-physical smoothness to the numerical solution.

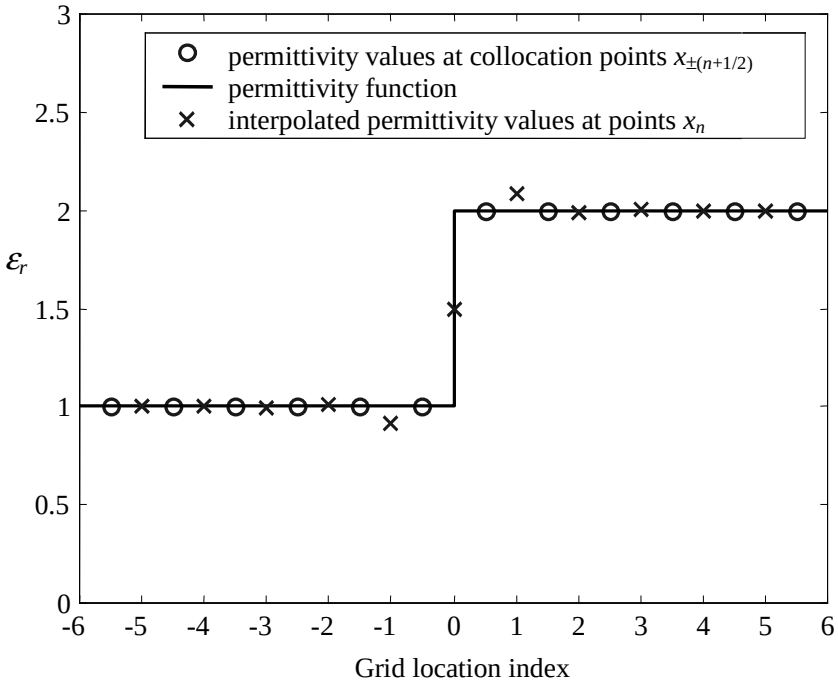

Figure 5. Smoothing of material discontinuity by implicit interpolation.

For 1-D problems, the implicit interpolation is a simple matter. Things get much more involved as the dimension of the problem increases. Especially in general 3-D problems, to find the interpolated material parameters, one has to solve a system of equations having essentially as many unknowns as there are field variables. Although the system is rather sparse, this may still be a prohibitive factor. Therefore, more research work is desired to find efficient ways to solve inhomogeneous problems using fourth-order algorithms.

2.3.5 Discussion

The high-order methods, especially the *Ty*-class methods, have been developed to reduce the large number of field variables in an FDTD simulation, while maintaining the accuracy. Of these methods, the *Ty*(2,4)-algorithm resembles most the standard FDTD scheme, using identical time stepping and same stencils for the spatial derivatives.

There are two main reasons to expect that the *Ty*(2,4)-algorithm (or any other so far known high-order method) will not replace the standard FDTD in general use. First, the grid parameter is frequently determined by geometrical considerations, not by the wave resolution, and therefore it may not be feasible to increase the cell size. If the wave resolution is already good, the use of a high-order method only increases algorithm complexity and code execution time. Other modeling approximations usually dominate the total error in such cases (see Section 1.3) and, hence, the improved accuracy will probably be covered by more dominating error sources. Second, compared to standard FDTD, a consistent treatment of discontinuous material parameters is much more elaborate, especially in 3-D problems.

The advantages of the high-order methods, when feasible, are undisputable. Therefore, related research work of the CEM community is desired to find out how these advantages could best be exploited.

2.4 Reduction of numerical dispersion in FDTD

2.4.1 Numerical dispersion as a measure of accuracy

Numerical dispersion and dissipation are characteristic properties of any finite difference algorithm for wave-like equations. They describe how the algorithm preserves waveform shapes. Qualitatively, for a pulsed waveform, dissipation appears as smoothening and dampening of the waveform, while dispersion appears as widening of the pulse; numerical anisotropy causes spherical waveforms to become slightly cubical. FDTD algorithm is conservative which means that no dissipation is introduced by the algorithm itself. Therefore, numerical dispersion alone describes the wave transport properties of the FDTD algorithm. To the author's understanding, dispersion error is the best problem-independent measure of the accuracy of FDTD. One must note, however, that good wave transport quality does not necessarily imply good ability to manage field singularities or some other peculiarities, but at least the contrary holds: poor transport quality implies practically always poor accuracy in any measure. Therefore, small dispersion error is a necessary condition of a useful algorithm.

2.4.2 Low-dispersion algorithms

In the research community, effort has been made in developing low-dispersion FDTD algorithms. In [36], several of the recent approaches are compared, including [32,37-41]. The method in [37] is based on wavelet expansions while [38] involves a high-order method similar to [32]. Paper [39] introduces a modified finite difference operator where the approximation error is minimized at a given design frequency. Paper [40] and a subsequent paper [42] present an FDTD algorithm involving two overlapping grids, resulting highly isotropic dispersion characteristics of the lattice. Paper [41] involves an error cancellation

procedure quite similar to [P1], which is discussed in more detail in Section 2.4.3. In [8, Chapter 4], Gedney *et al.* show that numerical *anisotropy* can greatly be reduced by using triangular mesh, instead of rectangular.

Especially innovative is the so-called pseudospectral time-domain (PSTD) method by Liu [43], where the spatial derivatives are computed using FFT. The dispersion error is entirely controlled via the size of the time step, and is reduced asymptotically faster than any polynomial of Δt. Using perfectly matched layers (PML), Liu has circumvented problems associated to the inherent assumption of periodicity of the structure, thus making the method much more attractive. The spatial resolution in PSTD can be dropped to the Nyquist limit, i.e. two cells per wavelength. The method itself needs further development to properly model material inhomogeneities. An attractive application of PSTD could be the evaluation of field distribution in a large 3-D domain – say in an office room – due to a radiating source. Such studies have been performed for 2-D building models using a high-order FDTD [38].

2.4.3 Reduction of numerical dispersion through anisotropy

As argued in Section 2.3.5, it seems probable that the basic FDTD algorithm will be generally used also in the future, despite the new algorithms. The standard way to control numerical dispersion is via the density of the grid. Paper [P1] describes a new approach to partially compensate the dispersion error. It is demonstrated in [P1] that unequal grid resolution along different coordinate directions ($\Delta x \neq \Delta y$) influences numerical dispersion significantly. In such cases the proposed reduction scheme provides most remarkable improvement.

In the following, we separate conceptually numerical dispersion into numerical anisotropy (direction dependence) and actual dispersion (frequency dependence).

The starting point in the study [P1] is that an FDTD lattice resembles anisotropic medium, because the phase velocity depends on direction. Note, however, that this is not the only property of anisotropic media. In general, each direction in an anisotropic medium supports two different propagation velocities, corresponding to two eigenpolarizations. Thus, an arbitrary wave will be split into two independent wavefronts in anisotropic medium [44].

The following question arises: is it possible to choose the *medium* anisotropy parameters such that the *numerical* anisotropy would be cancelled, and the resulting model would represent isotropic free space? It turns out that in a sense optimal anisotropy parameters can easily be found for fixed frequency, requiring only few lines of Matlab for a 3-D problem, given in the Appendix (code “comp3d”). The eigenpolarization splitting can simply be avoided by setting the relative permittivity and permeability tensors equal [P1]. The cancellation has been realized via diagonal anisotropy tensors; the anisotropy parameters appear in only a few update constants. In other words, the cancellation does not increase the computational burden.

Unfortunately, perfect cancellation is not possible with this approach. However, the parameters are designed such that the maximum dispersion error is minimized over all angles of propagation, and the average error over all angles is approximately zero. Therefore, an additional possibility to error cancellation via reflections takes place.

Closer examination reveals that deviation from cubical cell shape makes the dispersion error much larger. As an example, let us consider a 2-D problem. Let us define the grid resolution measure as the square root of the number of cells per area in units of λ^2, or

$$\hat{R} = \lambda / \sqrt{\Delta x \Delta y}. \tag{19}$$

Note that a non-standard resolution measure is used in [P1]. Here, instead, $\hat{R}$ reduces to the standard resolution measure if $\Delta x = \Delta y$. Table I shows the maximum dispersion error for $\hat{R}$ = 10 and a number of different cell shapes. The maximum error using the dispersion reduction and an error reduction factor are also given. Table II shows corresponding numbers for $\hat{R}$ = 20. It is obvious that the reduction is most significant for highly deformed cells.

TABLE I. Maximum dispersion error with and without dispersion reduction as a function of cell shape for fixed grid resolution $\hat{R}$ = 10. Stability coefficient = 0.99.

$\Delta x/\Delta y$	max error without reduction	max error with reduction	Error reduction factor
1	0.87 %	0.42 %	2.06
2	2.82 %	0.53 %	5.32
3	4.91 %	0.72 %	6.86
4	7.10 %	0.92 %	7.69
5	9.45 %	1.14 %	8.27

TABLE II. Maximum dispersion error with and without dispersion reduction as a function of cell shape for fixed grid resolution $\hat{R}$ = 20. Stability coefficient = 0.99.

$\Delta x/\Delta y$	max error without reduction	max error with reduction	Error reduction factor
1	0.21 %	0.10 %	2.04
2	0.67 %	0.13 %	5.18
3	1.14 %	0.17 %	6.57
4	1.60 %	0.22 %	7.21
5	2.05 %	0.27 %	7.55

A few 3-D examples given in [P1] demonstrate that the reduction parameters improve the accuracy in a reasonable band around the design frequency. Surprisingly, simulation experiments suggest that the optimal design frequency should be at the *low* end of the desired band, instead of center. It can be shown that if one designs the reduction parameters at frequency f_0, then the maximum dispersion error at *all* frequencies *higher* than f_0 will be less than in the standard FDTD. Towards lower frequencies, however, below a certain frequency, the standard FDTD will eventually have less error. This explains qualitatively the above experimental observation.

Inhomogeneous problems can also be treated straightforwardly. The change of wavelength and Courant-number in different dielectrics has to be taken into account, but otherwise the reduction parameters are simply averaged at material interfaces.

3 Absorbing boundary conditions in FDTD

Virtually all FDTD simulations require use of absorbing boundary conditions (ABC). Therefore, being of fundamental importance, it is natural that the subject has been under widespread examination from the early days of FDTD. In the following sections, we briefly review the most common ABCs, paying special attention to the perfectly matched layer (PML) and the original work contained in this thesis.

Some practical cases, where ABCs are not needed, are the following: a) 1-D simulations, since the computational volume can usually be made sufficiently large to prevent any reflections from the outer boundary to interfere with the solution region; b) closed resonators and c) compact 2-D FDTD waveguide models [16].

3.1 Traditional local ABCs

Next, we list the traditional local ABCs used in FDTD, and highlight some of their properties. The listing follows the guidelines given in [45, Chapter 7] in condensed form. The so-called global ABCs never enjoyed much popularity in FDTD, because they involve very expensive integration of fields during each time step.

3.1.1 Bayliss-Turkel ABC

The Bayliss-Turkel ABC [46] can be applied most naturally in spherical coordinates. Technically, it is a differential operator that annihilates a number of terms in a series expansion of the outgoing field. The form of the annihilator resembles that of the Sommerfeld radiation boundary condition, but the Bayliss-Turkel operators are enhanced to annihilate not only $1/r$-terms, but also higher-order terms. The order of the operator can be taken as a parameter. Usually a second-order operator is used, providing remainder terms of the order $1/r^5$.

With moderate modifications, the Bayliss-Turkel operator can be applied also in cylindrical coordinates, but unfortunately the application in Cartesian coordinates is not feasible. The practical realizations are reported to provide reflections on the order of –40 dB [45].

3.1.2 Engquist-Majda operator and Mur ABC

Engquist and Majda developed a famous pseudodifferential operator allowing wave propagation in only one direction [47]. Theoretically, the ABC based on Enquist-Majda operator is perfect for dispersionless media. The difficulty lies in the realization of the pseudodifferential operator. Many subsequent practical ABCs involve different approximations of the operator

$$\sqrt{1-S^2}, \text{ where } S = c\,\partial_s / \partial_t . \tag{20}$$

Above, c is the speed of light, and s represents x, y or z. Approximating (20) by polynomials of S results in realizable algorithms. The simplest approximations are based on Taylor

expansion, and efficiently implemented in FDTD by Mur [22]. The second-order Mur is a notable simple ABC and a preferred choice if extremely good absorption is not crucial.

3.1.3 Trefethen-Halpern ABC

Basically, the proposition of Trefethen and Halpern [48] is just a more general approximation of (20) via rational functions. Such an approximation can be chosen to interpolate (20) at a number of points. It turns out that these points correspond to certain incident-wave angles, where perfect absorption is theoretically obtained. One can increase the number of the exact absorption angles by making the approximation order higher. However, a high-order approximation results in increased algorithm complexity.

Trefethen-Halpern ABC has been tested in actual numerical experiment [45], revealing that the theoretical performance is not realizable. Moving from second-order algorithm to a third-order one improves the absorption, but not significantly. It seems that reflection level of about 1 % cannot be made smaller using this approach, probably due to numerical dispersion.

3.1.4 Higdon ABC

Higdon differential annihilator [49] is designed to annihilate a set of propagating plane waves. Higdon demonstrated that his operator is a further generalization of the Trefethen-Halpern operator. In Higdon method, the angles of exact (theoretical) absorption are set by the user as principal parameters. A distinct merit of Higdon ABC is that the FDTD realization involves only stencils normal to boundaries. This considerably simplifies the more involved Trefethen-Halpern ABC.

Unfortunately, the realized reflection level of Higdon ABC is of the same 1 % order than obtained using the previous methods. There is one promise, however, to improve Higdon ABC: the differential operators involve explicitly phase velocity of waves. If one uses the numerical phase velocity, determined by the numerical dispersion relation, the performance could possibly be enhanced.

3.1.5 Liao extrapolation

Another proposition for an ABC is given by Liao *et al*. [50]. As interpreted in [45], the Liao ABC can best be understood as a simple extrapolation of the fields inside the computational domain to the outer boundary. In the extrapolation, several time levels and several spatial points inside the computational domain are involved to efficiently perform the extrapolation. The extrapolated value is then used in normal manner in the update equations.

In numerical simulations, Liao ABC is seen to fulfill its theoretical performance better than Trefethen-Halpern or Higdon ABCs. The reflectivity of a three-time-level Liao ABC is reported to be much less than any of the computationally comparable versions of the other ABCs discussed so far, and about 20 dB less than second-order Mur [45].

3.1.6 Mei-Fang superabsorption

Mei and Fang proposed a method [51] to enhance the absorption of any existing local ABC. In other words, they did not propose a new ABC, but described an error cancellation procedure that involves application of the underlying ABC (Mur, Higdon or Liao, for example) to both electric and magnetic fields on the outer boundary. Due to the similar action of the ABC for both field components, this action can be extracted and cancelled. Mei and Fang reported about 10 dB typical enhancement in the reflectivity of the underlying ABC.

3.1.7 Conclusion

Concluding, the classical ABCs applied in FDTD give a reflection level roughly 0.5 %…5 %. To be comparable with high-quality anechoic chambers, an enhancement of at least 40 dB is necessary. Until the invention of the perfectly matched layer, to be discussed next, this limitation was among the most severe concerning FDTD simulations. Note that numerical dispersion in part seems to prevent advantageous use of high-order local ABCs. The ABCs based on differential operators had really reached a deadlock.

3.2 Perfectly Matched Layer (PML)

The idea of a perfectly matched layer originates most probably from the physical absorbers commonly used in microwave engineering: the solution region is surrounded by properly designed lossy material layer. As early as 1975 Taflove and Brodwin touched upon the ABC based on this concept [11], but at that time an absorption layer appeared too expensive in terms of computer storage. Also, Taflove and Brodwin realized the predictable problems related to impedance mismatch of free space and the absorbing layer. Berenger's far-reaching idea was to perfectly match a lossy layer to free space by splitting field components into two parts and non-physically associating independent conductivities to each part [23]. The discussion in this section follows the general lines drawn in the more comprehensive survey on PML given in [8, Chapter 5].

3.2.1 Original formulation

In 2-D TE case, the equations governing the original PML are the following [23]:

$$\varepsilon_0 \partial_t E_x + \sigma_y E_x = \partial_y (H_{zx} + H_{zy}), \tag{21a}$$

$$\varepsilon_0 \partial_t E_y + \sigma_x E_y = -\partial_x (H_{zx} + H_{zy}), \tag{21b}$$

$$\mu_0 \partial_t H_{zx} + \sigma_x^* H_{zx} = -\partial_x E_y, \tag{21c}$$

$$\mu_0 \partial_t H_{zy} + \sigma_y^* H_{zy} = \partial_y E_x. \tag{21d}$$

Here, the H_z-component has been split: $H_z = H_{zx}+H_{zy}$. The cornerstone of the whole PML is that σ_x^* and σ_y^* can be chosen independently. If they were constrained to be equal, Equations (21c) and (21d) could be merged, resulting ordinary Maxwell's equations with magnetic conductivity. Note that Equations (21a)-(21d) allow direct implementation with FDTD.

A PML can conveniently be parametrized by the set $(\sigma_x, \sigma_x^*, \sigma_y, \sigma_y^*)$. Vacuum is a special case, namely (0,0,0,0). Berenger showed in [23] that a PML is perfectly matched to vacuum at an interface normal to *x*-direction, i.e. producing no reflection from the interface at any angle of incidence and any frequency, provided it is of the form $(\sigma_x, \sigma_x^*, 0, 0)$, and the matching condition

$$\sigma_x / \varepsilon_0 = \sigma_x^* / \mu_0 \tag{22}$$

is fulfilled. At an interface normal to *y*-direction, matching is obtained by a medium $(0, 0, \sigma_y, \sigma_y^*)$, provided the conductivities again satisfy a similar condition than (22).

Berenger's original paper involved only 2-D case; PML was soon generalized into 3-D [52]. Being revolutionary, PML has attracted a lot of attention by several researchers and research groups. Since its first publication, hundreds of PML-related articles have been published.

3.2.2 Stretched-coordinate formulation

For theoretical examinations, a more compact form of the PML in terms of the so-called stretched coordinates was given by Chew and Weedon [53] and Rappaport [54]. Although the PML equations appear in a non-split form in the stretched-coordinate formulation, it cannot be directly implemented in FDTD, because the new coordinates are frequency-dependent. However, the advantage of the formulation lies in the unified appearance with the Maxwell's equations, helping subsequent mathematical manipulations related to e.g. developing PML for other coordinate systems. As well, the complex-coordinate representation can directly be utilized in frequency-domain algorithms.

3.2.3 Uniaxial formulation

A popular formulation of PML is the so-called uniaxial formulation [55]. In this formulation, PML is realized through an anisotropic medium having complex permittivity and permeability tensors. It is shown in [55] that if the tensors of the uniaxial medium have the form

$$\overline{\overline{\varepsilon}} = \varepsilon_0 \mathrm{diag}(s_x^{-1} s_y s_z, s_x s_y^{-1} s_z, s_x s_y s_z^{-1}), \qquad \overline{\overline{\mu}} = \mu_0 \overline{\overline{\varepsilon}} / \varepsilon_0, \tag{23}$$

where s_x, s_y and s_z are any complex numbers, then a plane wave experiences no reflection from any vacuum/medium interface, independent of frequency or angle of incidence. By proper choice of s_x, s_y and s_z, a medium characterized by (23) is frequently called uniaxial PML or UPML. The corresponding choice is

$$s_x = 1 + \sigma_x / (j\omega\varepsilon_0), \quad s_y = 1 + \sigma_y / (j\omega\varepsilon_0), \quad s_z = 1 + \sigma_y / (j\omega\varepsilon_0). \tag{24}$$

UPML has essentially the same properties than Berenger's split-field PML. Strictly speaking, UPML is uniaxial only in regions where the absorbing layers do not overlap. Note also that the fields are unsplit in UPML, but the parameters are frequency-dependent.

There is an additional useful degree of freedom in UPML: one can increase the real parts of the parameters s_x, s_y and s_z in order to *enhance evanescent wave attenuation*, without destroying the perfect matching [8, Chapter 5.5]. In standard PML, evanescent waves are not attenuated.

In FDTD realization of UPML, the apparent memory advantage of unsplit formulation is compensated by the need to introduce auxiliary variables to handle frequency-dependent parameters. Auxiliary variables can be avoided by introducing time-dependent source terms [56]. For typical simulation cases, a memory saving of about 25 % is obtainable, as compared to split-field PML [56]. However, if memory is not a very critical factor, it is recommended for ease of programming to introduce the auxiliary variables in the whole computational space and double the memory requirement, exactly as in split-field PML.

To the author's opinion, from FDTD point of view, the most significant improvement of UPML over split-field PML is the promise for evanescent wave attenuation.

3.3 Optimization of the conductivity profile in PML

While implementing PML in FDTD, one is faced with the fact that too sudden increase of the conductivity in the layer causes high reflections, although the continuous model allows in principle arbitrary high absorption in arbitrary thin layer. Because the conductivity profile can be freely chosen by the user, the question of profile optimality is reasonable.

3.3.1 Widely used conductivity profiles

Based on experiments, it was realized from the beginning [23] that the conductivity must vary smoothly in FDTD implementation; otherwise reflection level increases. To find a balance, Berenger proposed a polynomial variation of the conductivity in the layer [23]:

$$\sigma(\rho) = \sigma_m \left(\rho / \delta\right)^n, \tag{25}$$

where δ is the thickness of the layer and ρ is the distance from the vacuum/PML interface. The resulting theoretical reflection coefficient for a plane wave with angle of incidence θ is

$$R(\theta) = \exp\left(-(2\sigma_m \delta \cos\theta)/(\varepsilon_0 c(n+1))\right). \tag{26}$$

Subsequently, exponential profile has also been suggested [57]. There are at least two reasons for using such profiles. First, for a given thickness, the profile is expressed by only two parameters (σ_m and n), and second, one can estimate the reflection from PML using the continuous model. Typically, PML thickness is 4-16 cells and theoretical normal reflection coefficient is –80 dB. However, Equation (26) is useful only if the layer is thick enough and the theoretical reflection high enough. For example, choosing $R(0)$ = –150 dB for a 2-layer PML yields actually very poor performance.

We put the problem as follows: for a given layer thickness, what is the least obtainable reflection level in an FDTD realization? With which profile this optimum is obtained? Previous studies about this question restrict the optimization to polynomial profiles only; in

effect, parameters σ_m and n are optimized [57-65]. However, there is no reason to expect that the arbitrary choice of polynomial or exponential profile is optimal. The optimization problem is discussed in paper [P2] from more general standpoint.

3.3.2 Closed-form expression for the reflection in 1-D FDTD

The efficient profile optimization is based on an analytical formula relating discrete conductivity values in PML and the reflection coefficient. The formula and its use are described in [P2], but due to limited space in [P2], the derivation of the formula for 1-D case is presented here. We analyze only the simplest 1-D case in detail; the general case follows by recursion.

So, let us have a 1-D PML containing just one location where conductivity is nonzero, Figure 6. Here and in the following, PML is assumed to be backed by PEC.

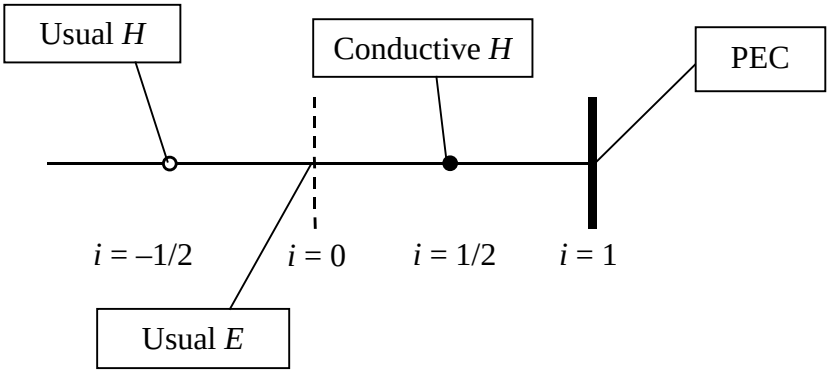

Figure 6. The simplest 1-D PML.

In a steady-state situation, incident and reflected waves can be written as Fourier-modes (outside the PML region):

$$V_{inc,i}^{n} = V_{inc} e^{j(\omega n\Delta t - ki\Delta x)}, \tag{27}$$

$$V_{ref,i}^{n} = V_{ref} e^{j(\omega n\Delta t + ki\Delta x)}. \tag{28}$$

Here, V stands for both electric and magnetic fields. We agree the signs such that positive E_{ref} means opposite field to positive E_{inc}. Thus, the total field is $E_{tot} = E_{inc} - E_{ref}$. For the magnetic field, $H_{tot} = H_{inc} + H_{ref}$. Assuming free space, the discretized one-dimensional Maxwell's H-equation at point $i = 1/2$ takes the form

$$\mu_0 D_t H_{1/2}^{n+1/2} + \sigma^H H_{1/2}^{n+1/2} = -D_x E_{1/2}^{n+1/2}, \tag{29}$$

where D_t and D_x are temporal and spatial centered finite difference operators, respectively. The update step for $H_{1/2}^{n+1/2}$ is

$$\left(H_{1/2}^{n+1} - H_{1/2}^{n}\right)/\Delta t + (\sigma^H / 2\mu_0)\left(H_{1/2}^{n+1} + H_{1/2}^{n}\right) = -\left(E_1^{n+1/2} - E_0^{n+1/2}\right)/(\mu_0 \Delta x). \tag{30}$$

Using the PEC-condition ($E_1^{n+1/2} = 0$ for all *n*), and the assumed time-dependence $e^{j\omega n\Delta t}$, we have

$$\left[2j\sin(\omega\Delta t/2)/\Delta t + \sigma^H \cos(\omega\Delta t/2)/\mu_0\right] H_{1/2}^{n+1/2} = E_0^{n+1/2}/(\mu_0\Delta x). \tag{31}$$

Next, we introduce the Courant-number *Q* and the resolution parameter *R*:

$$Q = c_0\Delta t/\Delta x, \quad R = \lambda/\Delta x, \tag{32}$$

where λ is the wavelength in free space. It follows that

$$\omega\Delta t = 2\pi c_0\Delta t/\lambda = 2\pi Q/R. \tag{33}$$

Also the conductivity is normalized:

$$\sigma^N = \sigma^H \Delta x/\eta_0 . \tag{34}$$

Here, $\eta_0 = \sqrt{\mu_0/\varepsilon_0}$. To simplify notations, let us define the following parameters:

$$W = 2\sin(\pi Q/R)/Q, \tag{35}$$
$$S = \sigma^N \cos(\pi Q/R), \tag{36}$$
$$T = S + jW. \tag{37}$$

Now, (31) can be rewritten as

$$\eta_0 H_{1/2} = E_0/T. \tag{38}$$

The time dependence has been cancelled as a common term. At point *i* = 0 there are both incident and reflecting waves, and the *E*-equation becomes:

$$\begin{aligned} &\varepsilon_0 D_t\left(E_{inc,0}^n - E_{ref,0}^n\right) = -D_x H_0^n \Rightarrow \\ &jW\left(E_{inc,0}^n - E_{ref,0}^n\right) = \eta_0\left(H_{-1/2}^n - H_{1/2}^n\right). \end{aligned} \tag{39}$$

Again, we cancel the time dependence. Inserting (38) into (39), we get

$$jW\left(E_{inc,0} - E_{ref,0}\right) = \eta_0\left(H_{inc,-1/2} + H_{ref,-1/2}\right) - \left(E_{inc,0} - E_{ref,0}\right)/T . \tag{40}$$

Since $H_{-1/2}$ is outside the PML region, it can be decomposed into incident and reflected waves. Taking the sign agreement into account, the relation between H_{inc}, H_{ref} and E_{inc}, E_{ref} is:

$$\eta_0 H_{inc,-1/2}^n = E_{inc,-1/2}^n \quad \text{and} \quad \eta_0 H_{ref,-1/2}^n = E_{ref,-1/2}^n. \tag{41}$$

Using (27) and (28),

$$E^n_{inc,-1/2} = E^n_{inc,0} e^{jk\Delta x/2}, \qquad E^n_{ref,-1/2} = E^n_{ref,0} e^{-jk\Delta x/2}. \tag{42}$$

Combining (40) with (41)-(42), canceling again the time dependence, we get

$$jW\left(E_{inc,0} - E_{ref,0}\right) = E_{inc,0} e^{jk\Delta x/2} + E_{ref,0} e^{-jk\Delta x/2} - \left(E_{inc,0} - E_{ref,0}\right)/T\ . \tag{43}$$

We define reflection coefficient $\rho := E_{ref,0} / E_{inc,0}$. Rearranging (43), we finally have

$$\rho = (U - e^{jk\Delta x})/(1+U), \text{ where} \tag{44}$$

$$U = e^{jk\Delta x/2}\left(jW + 1/T\right). \tag{45}$$

The general formula is similar, only U takes a form of a continuous fraction [P2]. A Matlab-program "rho_1d" is given in the Appendix, evaluating ρ for parameters Q, R and normalized conductivity values σ^N.

3.3.3 Closed-form expression for the reflection in 2-D FDTD

The 2-D case can be analyzed similarly than the 1-D case, proceeding from the outer PEC boundary towards vacuum/PML interface. The formula obtained this way takes explicitly into account numerical dispersion in 2-D grid, and in all performed simulations it is observed to predict the reflection exactly within computer arithmetic accuracy.

We do not repeat the analysis, but merely give the reflection formula. Let us consider an M-layer PML normal to x-direction, defined by $2M+1$ conductivity values. We choose an odd number of conductivity values, because in that way the reflection formula is simpler. This is not restrictive, since we can join $\sigma = 0$ to the profile if desired.

Given the propagation direction α, frequency f, and the grid parameters Δx, Δy and Δt, we define the following parameters to simplify notations later:

$$Z = \Delta x/\Delta y, \quad Q_2 = \sqrt{1+Z^2}\, c_0 \Delta t/\Delta x, \tag{46}$$

$$R_2 = \lambda/\sqrt{\Delta x^2 + \Delta y^2} = c_0/(f\sqrt{\Delta x^2 + \Delta y^2}), \tag{47}$$

$$\tilde{W} = \pi Q_2 Z/(R_2(1+Z^2)), \quad W = 2\sqrt{1+Z^2}\sin(\tilde{W})/Q_2, \tag{48}$$

$$\left.\begin{aligned} S_i &= \sigma_i^N \cos(\tilde{W}) \\ T_i &= S_i + jW \end{aligned}\right\}, \quad i = 1,\ldots,2M+1. \tag{49}$$

Q_2 is the Courant-number and R_2 is a resolution parameter. Z is simply a cell-shape parameter, and has nothing to do with impedance. The normalized conductivity values σ_i^N are defined as follows:

$$\sigma_i^N = \begin{cases} \sigma_i^H \Delta x / \eta_0 \text{ at magnetic field location,} \\ \sigma_i^E \Delta x \eta_0 \text{ at electric field location.} \end{cases} \tag{50}$$

In addition, we need the numerical wave vector $(k_x, k_y) = k(\cos(\alpha), \sin(\alpha))$, which is obtained from the numerical dispersion relation (16). Having solved *k*, we proceed defining

$$\begin{aligned} P &= 4Z^2 \sin^2\left(k\Delta y \sin(\alpha)/2\right)/W^2, \\ Y_i &= \begin{cases} T_i(1-P) \text{ if } i \text{ is odd,} \\ T_i \text{ if } i \text{ is even.} \end{cases} \quad i = 1,\ldots,2M+1 \end{aligned} \tag{51}$$

$$U = 2e^{jk\cos(\alpha)\Delta x/2} \sin\left(k\Delta x \cos(\alpha)/2\right)\left(jW + \left(Y_1 + \left(Y_2 + \ldots + Y_{2M+1}^{-1}\right)^{-1}\right)^{-1} \right)/W. \tag{52}$$

The reflection coefficient is finally

$$\rho = (U - e^{jk\cos(\alpha)\Delta x})/(1+U). \tag{53}$$

A Matlab-program "rho_2d_exact" is given in the Appendix, evaluating ρ for given parameters α, Z, Q_2, R_2 and normalized conductivity values σ^N.

3.3.4 New proposition for the conductivity profile design

One may consider optimizing the profile by first defining a proper norm for the reflection over wide frequency band and wide selection of angles, and then minimizing (53) in that norm over all $2M+1$ normalized conductivity values. There are efficient multi-dimensional optimization algorithms available, for example the Hooke-Jeeves line search algorithm [66]. Note that the dimension of the optimization problem is not very large, of the order of 10 - 40.

We propose, however, another approach. Equation (53) reveals immediately that zero reflection is possible, namely if $U = e^{jk\cos(\alpha)\Delta x}$. For one set of wave and grid parameters (α, f, Δx, Δy, Δt), the zeroing condition defines two equations for U:

$$\mathrm{Re}(U) = \cos(k\cos(\alpha)\Delta x), \tag{54}$$

$$\mathrm{Im}(U) = \sin(k\cos(\alpha)\Delta x). \tag{55}$$

Thus, M wave and grid parameter sets define $2M$ equations to be satisfied by U. Since we assume $2M+1$ normalized conductivity values, to be considered as independent variables of U, we expect that M zeroing equations can be satisfied. The additional degree of freedom can be "spent" at zero frequency, because at f=0, Equation (55) is trivially satisfied.

For given grid parameters, we propose designing PML by selecting M pairs (f_i, α_i) (and possibly a pair (0, α_0)). Then some numerical technique is applied to solve σ^N, such that zero reflection is obtained for the corresponding plane waves. Next, the reflection at other frequencies and angles of incidence is evaluated. If the result is not satisfactory, the design parameters (f_i, α_i) are changed, and new conductivity values are solved.

To find the solution of the zeroing conditions, a multi-dimensional Newton iteration has been tested and found otherwise efficient, except that a good initial guess is required. In a recent paper [65], it is suggested to treat 2-D wave essentially as a 1-D wave propagating with velocity $c_0/\cos(\alpha)$. We explored this approach, and found the resulting simple formula satisfactory in all cases studied. A Matlab-code "rho_2d" based on 1-D formula is given in the Appendix. The results of "rho_2d" are essentially the same than that of "rho_2d_exact". The evaluation of "rho_2d" is simpler and faster, and therefore it is a preferred code to be used in either Newton iteration or some other iterative solution of the zeroing conditions.

Furthermore, it seems reasonable to expect that a 3-D PML problem can also be reduced to a 1-D problem. For time being, however, we do not have numerical results verifying this claim.

Paper [P2] gives some examples about the advantages obtainable by the optimization. In a parallel-plate waveguide problem, just four-layer PML can be designed to yield reflection less than –82 dB for the dominant mode over a band 1.33 f_c…3.22 f_c, as compared to –54 dB reflection of an optimal polynomial profile of the same thickness. There remains problem at cut-off, a subject deserving further development. The promises of evanescent wave attenuation of UPML mentioned in Section 3.2.3 (and applied in e.g. [67]) point towards a preferred direction of development of the present theory.

An optimized PML should be especially useful in scattering problems employing total/scattered field formulation [22,68], because only the scattered field needs to be absorbed, and it is usually much more radial than the total field. This would make almost problem-independent optimization of PML profiles feasible.

3.4 Ramahi's complementary operators method (COM)

A recent advancement in ABC theory is Ramahi's Complementary Operators Method (COM) [69]. Like Mei-Fang superabsorption scheme, COM is not an ABC by itself, but is an error cancellation procedure associated to a 'host' ABC, especially to that of Higdon. There is evidence that COM can be made comparable or superior to PML [70]. COM is reported to provide naturally absorption of both propagating and evanescent waves.

Despite being very interesting in principle, COM is not studied further in this thesis.

4 Coupling probe models in FDTD

In microwave engineering, many devices of practical interest involve coupling of electromagnetic energy via an extension of the inner conductor of a coaxial cable, also called coupling probe. Probes can be used as monopole-type antennas, they might be bended to form a coupling loop to a resonator, or they may contact a metal patch to feed a special antenna. Probes are also commonly used to realize coaxial-to-waveguide or coaxial-to-stripline transitions [71,72]. Due to its relative universality, proper modeling of the coupling probe in FDTD is essential. Paper [P3] and Section 4.2 involve a generalization of a well-known probe model [19]. Before considering that, the practical value of FDTD in modeling an interesting antenna structure is discussed.

4.1 Simulation case: dielectric resonator antenna

In the Radio Laboratory, HUT, small-sized antennas are studied intensively. One of the promising candidates to be used in wide-band mobile telecommunications is the half volume dielectric resonator antenna (DRA) [73,74,P3]. A dielectric resonator is basically a piece of high-ε_r material. FDTD can be utilized efficiently in the design of DRAs. The size, shape and ε_r of a DRA can easily be varied in simulations. Visualization helps understanding resonance phenomena in the DRA. For example, Figures 7a and 7b depict snapshots of the electric fields in model 1) of [P3]. Snapshots are taken on the symmetry plane at center frequencies of the first and second resonances.

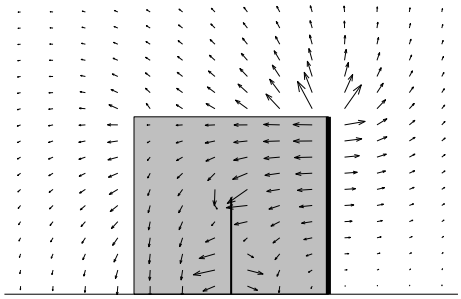

Figure 7a. First resonance at 2.159 GHz.

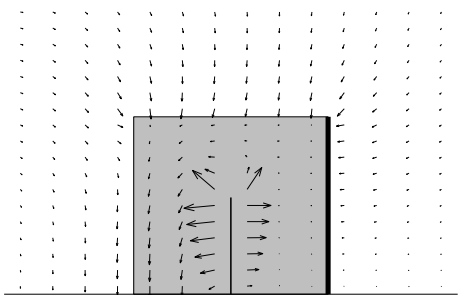

Figure 7b. Second resonance at 3.900 GHz.

The figures above, and especially the related ‘movies’ obtained from a sequence of snapshots, help understanding operation of the antenna. For the programmer, a quick look at such a figure is a qualitative test for the code. Above, for example, we can inspect that the electric field is normal to the short circuit (the thick vertical line) and to the ground plane (bottom horizontal line).

We understand from Figure 7a the shape of the first resonance mode, and that the field has a hot spot on top of the short circuit. Figure 7b tells us that the second resonance mode resembles quarter-wave monopole resonance, and that significant portion of the electromagnetic energy is concentrated near the probe. These facts explain why the second resonant frequency depends crucially on the length of the probe and on the air gap between

the probe and the dielectric; the former is obvious, and the latter is due to high energy density in the air gap – a small change in the air volume affects significantly the energy distribution in the whole system, and sensitivity to dimensions of the air gap is expected. A sequence of simulations can be selected to quantify the sensitivity analysis.

4.2 Generalized model of a coaxial probe

The coaxial probe model of Maloney [19] assumes that $\Delta x = \Delta y = \Delta$, and that the radius of the outer conductor of the coaxial cable (r_o) equals Δ. Quite often, proper modeling of the dimensions of the structure requires $\Delta x \neq \Delta y$. Assumption $r_o = \Delta$ is also restrictive, though it seems that small variations in the physical size of the cable aperture do not play a significant role, if the ground plane area is large enough. More important is to model properly the radius of the inner conductor (r_i). A thin-wire model [75,76] is included in [19] and [P3]. In [P3], we have especially studied removing the restriction $\Delta x \neq \Delta y$.

Maloney's idea was to model the coaxial cable separately from the FDTD volume as a 1-D TEM-line, using the transmission line matrix (TLM) concepts. On the interface between the transmission line and FDTD grid, voltages and currents of the TLM are transformed into electric and magnetic fields of the FDTD, and vice versa. We retained this ideology, and made a simple generalization to Maloney's method: referring to Figure 8, the voltage/electric field transformation is performed at relevant locations in the FDTD grid (in the white area), using the known field distribution in the cable:

$$\vec{E} = \frac{V}{\ln(r_o / r_i)} \frac{1}{r} \vec{u}_r . \tag{56}$$

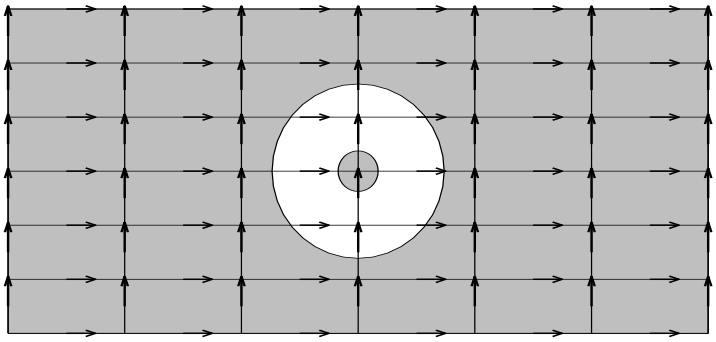

Figure 8. Cross-section of the coaxial cable in the aperture plane.

The only restrictions for the dimensions of the cable are: a) $r_i < \min(\Delta x/2, \Delta y/2)$ and b) $r_o > \max(\Delta x/2, \Delta y/2)$.

For comparison, we simulated the DRA of Section 4.1 using both our and Maloney's models. We modeled the cross-section of the DRA by 6×6 cells (the physical size of the cross-section is 8×17.5 mm^2), yielding Δx = 1.333 mm and Δy = 2.916 mm. To see if our model gives any improvement, we applied Maloney's model 'blindly', using the same grid. Since Maloney's model requires in principle $\Delta x = \Delta y = r_o$, our 'blind' application corresponds effectively to modeling a different r_o for x- and y-directions. Note, however, that r_i is modeled similarly in both models.

The results of the comparison are given in Figure 9. We see that our model predicts the width and location of the second resonance very well. Maloney's model predicts the bandwidth equally well, but there is a noticeable shift in the center frequency. The first resonance is associated mainly to the short circuit (see Figure 7a), and there is no essential difference between Maloney's method and ours. As pointed out in [P3], the second resonance is very sensitive to the air gap between the probe and the DRA. Because the discretization here is slightly different from that used in [P3], the air gap and the $|S_{11}|$-curve are also different from [P3]. However, the air gap is exactly the same in both simulations of Figure 9.

Concluding, the modification presented in [P3] removes the restriction $\Delta x = \Delta y$.

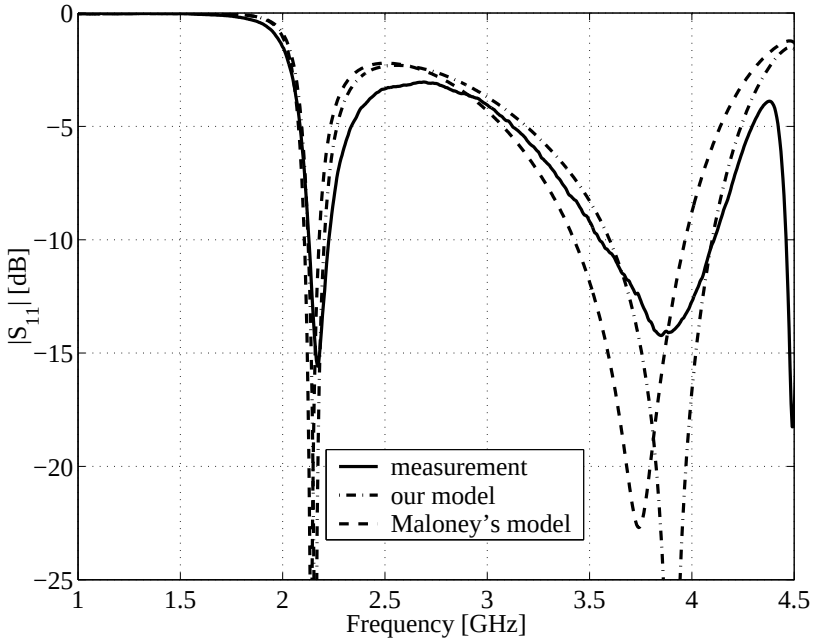

Figure 9. Comparison of our model and Maloney's coaxial probe model.

4.3 Resistive voltage source model

A simple alternative to the coaxial probe model is the widely used resistive voltage source (RVS) [2,21]. Paper [P4] pays special attention to two matters associated to RVS, namely the source impedance distortion due to cell capacitance, and dependence of input impedance Z_{in} on source cell height. The source impedance distortion can be avoided trivially, as explained in [P4], but the latter question deserves some comments.

A coaxial probe is normally realized using RVS in the following manner. The probe itself is modelled as a perfectly conducting wire, either using a thin-wire model or simply defining a row of PEC cell edges. The lowest cell in the probe is replaced by the RVS. In that cell, proper conductivity is defined resulting desired resistance of the cell, usually 50 Ω. The system is excited via E_z-component of the RVS cell, as described in [2].

If the probe height is N cells, the model consists of an N-1 cells high PEC structure and a one-cell RVS. One may justifiably ask, does the RVS form a part of the probe or not? Paper [P4] sheds some new light on this question.

One can try to answer the above question by making a straightforward test: fix a monopole length, and perform several simulations with varying Δz. The result is that Z_{in} is different in each case, see Figure 10. The obvious conclusion is that Z_{in} depends on cell height. This conclusion, however, is too straightforward.

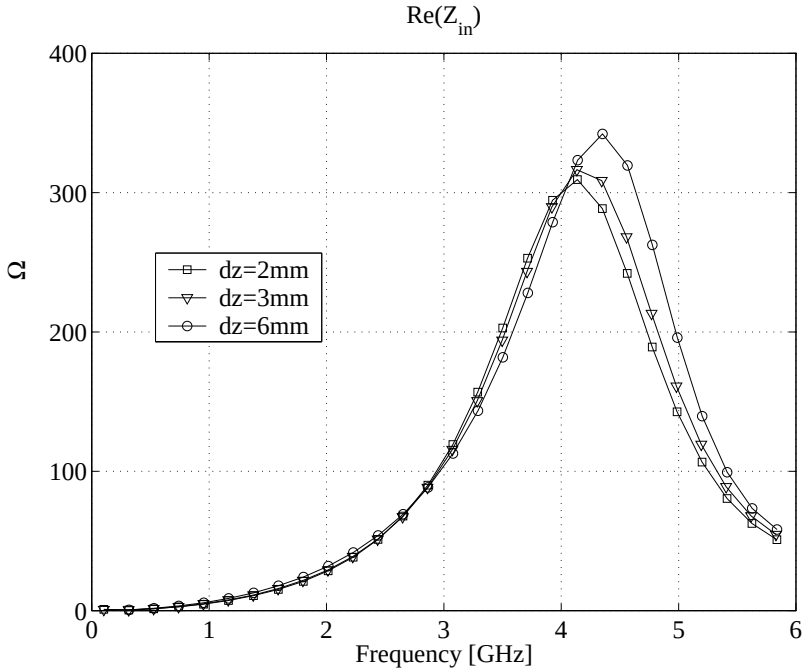

Figure 10. Real part of the simulated input impedance of a 30 mm monopole. $\Delta x = \Delta y = 5$ mm, Δz is shown in the legend.

We anticipate that the singular field on top of the monopole plays a significant role in the simulations. Variations in grid density result in different representations of the singular field, and we claim that the observed discrepancies in Z_{in} are primarily caused by this phenomenon. In other words, RVS is a part of the probe, and its height should not be compensated. The problem is not on bottom of the probe but on top of it.

It is well known by the users of FDTD that a PEC object looks effectively a bit larger than the geometry employed [13]. Therefore, to test our claim, we must choose a structure that eliminates the uncertainty related to both field singularity and effective size expansion. A structure satisfying fairly well the above criteria is depicted in Figure 11. The singularities near PEC corners are much less intensive than in the monopole example. Furthermore, the block on top of the monopole is thick enough to be modelled rather consistently, despite the effective expansion of its dimensions.

The results for three values of Δz are given in Figure 12, complementing the results of [P4]. Only real part of Z_{in} is plotted in order to keep the picture clear. We have assumed that the feeding point of the antenna is in the middle of the RVS cell, and transformed this point to the ground plane by multiplying the computed return loss S_{11} by $\exp(-j\omega\Delta z/(2c_0))$, and computing $Z_{in}^{cor} = Z_0(1+S_{11})/(1-S_{11})$. The curves in Figure 12 almost overlap, justifying our claim. Without reference point transformation, there would remain notable differences in Z_{in}.

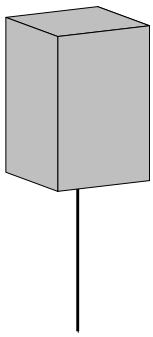

Figure 11. Sample structure used to test dependence of Z_{in} on Δz. The PEC piece on top of the monopole (height h = 30 mm) has dimensions $20\times20\times30$ mm^3.

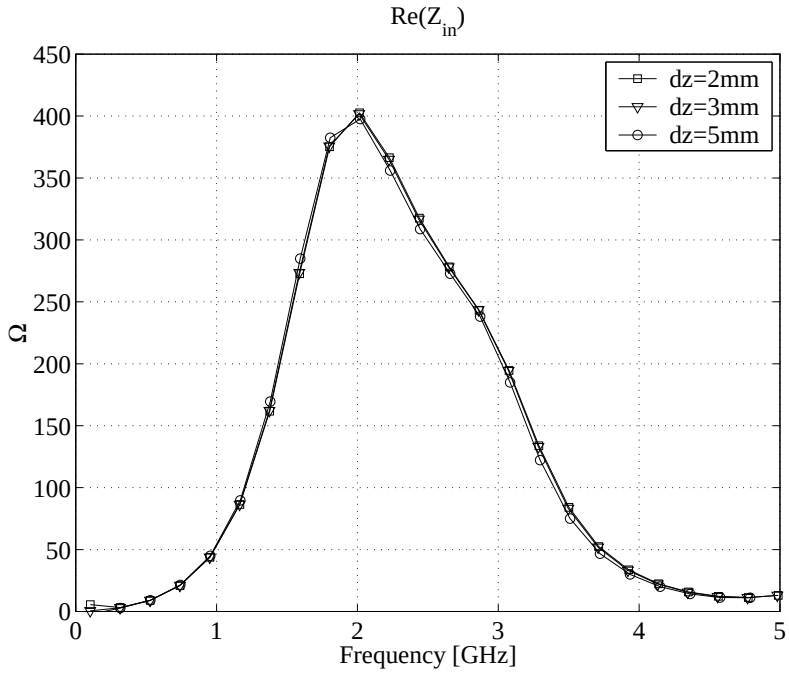

Figure 12. Real part of the simulated input impedance of the structure depicted in Figure 11. $\Delta x = \Delta y$ = 5 mm, Δz is shown in the legend. The feed point has been transformed a distance $\Delta z/2$ downwards in each case.

4.4 Improved thin-wire model

In a recent study [P5], the thin-wire model is studied further. The study covers so far only 2-D models. Here, we discuss briefly the reason why the standard model [75] is unsatisfactory. Novel propositions for the treatment of thin wires are also given in [77] and [78].

The treatment of a thin wire is based on the static solution: a static current in an infinite long wire produces a rotationally symmetric $1/r$ dependent circulating magnetic field, and a $1/r$ dependent radial electric field. We can assume similar $1/r$ dependence in the local neighborhood of the wire also in the time-varying case. Using this assumption and integral

form of Faraday's law, update equations for the magnetic fields surrounding the wire are obtained. The wire radius appears as a parameter in these equations.

This procedure is perfectly adequate. There is a problem, however, that is readily seen while considering the current flowing in the wire. In a symmetric case, the four magnetic field values looping the wire are equal, say H_0. Because H_0 represents rotationally symmetric magnetic field at a distance $\Delta/2$ from the center of the wire, the total loop integral of the magnetic field is $2\pi\cdot\Delta/2\cdot H_0$. However, conventional FDTD evaluation of the total loop integral of the magnetic field yields $4\cdot\Delta\cdot H_0$. In other words, conventional FDTD interpretation yields current that is a factor of $4/\pi$ too large. The same problem is met also in updating the adjacent axial electric fields. In short, the problem arises from mixing rotational symmetry and Cartesian grid. Figure 13 depicts this confusion.

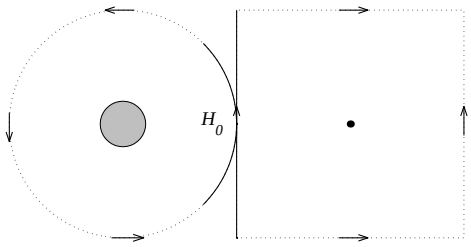

Figure 13. Ampere's law contour path in thin-wire model [75] (circular path) and in standard FDTD (square path). The gray patch represents the wire and the black dot the adjacent axial electric field location. The arrows looping the wire represent magnetic field components computed using the thin-wire update equations. One of these is used also in the square loop.

In updating the adjacent electric field (pointing outward from the paper), it is assumed that the magnetic field value H_0 in the middle of the solid vertical line represents the *average* of the field along that line. However, the $1/r$ assumption used in the thin wire model implies that H_0 is actually *maximum* of the field along that line. It is straightforward to calculate that the correct contribution to the line integral over the square loop is obtained by multiplying H_0 by the length of the 90^o arch, depicted in Figure 13, not by the cell edge length. This is in accordance with the requirement of consistent current evaluation.

Concluding, for a 2-D mesh with $\Delta x = \Delta y$, the magnetic field values obtained by the standard thin-wire algorithm must be multiplied by $\pi/4$ to obtain correct contributions to the magnetic field loop integrals in Ampere's law. If $\Delta x \neq \Delta y$, the correction factor is $(\Delta x/\Delta y)\tan^{-1}(\Delta y/\Delta x)$ at points $(\pm\Delta x/2,0)$ relative to the wire center, and $(\Delta y/\Delta x)\tan^{-1}(\Delta x/\Delta y)$ at points $(0,\pm\Delta y/2)$. In 3-D, the same confusion exists, but the solution is somewhat more involved, and is a current research topic. An important factor in 3-D is the field caused by the accumulated charge on top of a wire antenna.

4.5 Symmetry considerations and future work

The results of [P5] suggest that the thin-wire model in [P3] should be modified to accurately represent the probe diameter; unfortunately, the 3-D theory is still under development, and no comparisons are available yet. In addition to the inaccurate thin-wire model, there is an other shortcoming in both Maloney's and our coaxial probe model, namely both models assume that the electric field is rotationally symmetrical in the aperture of the cable. Both structures considered in [P3] have one plane of symmetry intersecting the cable aperture, so the assumption is somehow justifiable. Sample simulations and measurements with structures possessing no symmetry reveal that the coaxial probe model does not always work properly in such circumstances. The most probable explanation is the irrelevant symmetry assumption.

The symmetry assumption can be released by using the RVS model, Section 4.3. A possible disadvantage is that RVS neglects the dimensions of the aperture of the coaxial cable. Moreover, the z-directed electric field used in RVS, and also in the so-called delta-gap source [18], is non-physical. In practice, the RVS works well in many situations, but problems may arise, if there are interacting structures close to the aperture. In such case a non-physical coupling via the E_z-field may take place.

Another possible solution to improve the coaxial probe model would be looking some distance downwards the cable using FDTD, and assuming the TEM-mode far enough from the aperture. A modification of Maloney's model in this spirit is presented in [79], where the boundary between the transmission line and FDTD is half cell below the aperture, allowing non-symmetrical electric field in the aperture. It should be possible to move the boundary further downwards, using the methodology of [79].

A third possible option is using FDTD in cylindrical coordinates. Then, in the aperture, the cylindrical coordinates would be transformed into rectangular ones and vice versa. A coupled cylindrical and Cartesian grid has been used in [80]. A coaxial line study involving only cylindrical coordinates is presented in [81]. Here, only FDTD is used, and proper geometrical resolution inside the cable is obtained by dense subgridding. The reported results are very good, but assumed cylindrical geometry restricts the applicability of the method.

5 Finite Element Method

5.1 Introduction

The finite element method is one of the classical tools of numerical analysis, suitable for the solution of a wide class of partial differential or integral equations in almost arbitrary geometries. Traditionally, FEM was applied in mechanical engineering for structural analysis, starting from 1950's. Soon after that, FEM found applications also in electrical engineering. Apparently, the first application of FEM to the solution of cut-off wavenumbers of waveguides was reported in 1968 [82].

The mathematical theory of finite elements is deep and wide, and involves a great deal of functional analysis and especially Hilbert space theory. Several textbooks deal with the finite element mathematics, e.g. [83]. A comprehensive treatment taking especially electromagnetic aspects into account can be found in e.g. [84] and [85]. Due to the limited scope of this text, it is not possible to go into details; after a brief general introduction we outline the original work contained in this thesis in Sections 5.4 and 5.5.

As a numerical tool, FEM can be considered complementary to FDTD. Obviously, simulations with several independent methods provide higher degree of reliability. Some advantages of FEM as compared to FDTD are: 1) FEM is based on well-established mathematical theory, and the error control is somewhat more robust than in FDTD; 2) since FEM mesh is completely unstructured, complicated geometries can be modeled more accurately than in FDTD; 3) having fixed mesh, the user still has the freedom of selecting a proper basis (see Sections 5.2 and 5.3) and thus affecting the accuracy. This corresponds roughly to switching between 2^{nd}- and 4^{th}-order algorithms in FDTD, which is not a standard option.

5.1.1 Vector finite elements

In electrical engineering, the so-called vector finite elements [86-90] have emerged especially a) to enforce continuity of tangential components in material interfaces; b) to allow proper discontinuity of normal field components in material interfaces; c) to provide divergence-free solutions over the entire computational domain. Property c) is usually considered to be the key in avoiding the so-called spurious, non-physical solutions.

Vector FEM is particularly well suited for general inhomogeneous 3-D problems. However, compared to scalar elements, their construction is more cumbersome, especially if high-order elements are considered. Therefore, when feasible, scalar elements are preferred. This is the case in many 2-D problems, including e.g. many waveguide analysis problems. In homogeneous waveguides, TE and TM modes decouple, and a single field component suffices to describe each mode. Inhomogeneous waveguides, on the other hand, are properly solved in terms of transverse magnetic field, i.e. in terms of two scalar fields [91]. This assumes that the materials are non-magnetic. The solution is assured to have zero divergence, and spurious solutions are thus avoided.

Despite being a hot research topic, vector finite elements are not considered further in this thesis, but only scalar FEM is discussed.

5.1.2 Basic idea of FEM solution construction

First, we define the frequently used L_2- and H^1-norms of a function f defined on Ω:

$$\begin{aligned} \|f\|_{L_2} &= \int_\Omega f^2 d\Omega, \\ \|f\|_{H^1} &= \int_\Omega (f^2 + |\nabla f|^2) d\Omega. \end{aligned} \tag{57}$$

For example, the space $H^1(\Omega)$ is the collection of functions f defined on Ω having finite H^1-norm. Occasionally, we also use the concept of H^1-seminorm:

$$|f|_{H^1} = \int_\Omega |\nabla f|^2 d\Omega. \tag{58}$$

As explained in Chapter 2, FDTD is constructed such that Maxwell's equations are approximately satisfied at each grid point. FEM, instead, is based on global approach. Oversimplifying, the FEM solution is constructed such that the integral of the residual error between the exact and numerical solution is zero with respect to several weighting functions. Symbolically, if L is some linear operator (representing e.g. Helmholtz or Laplace operator), and f is a 'source' or 'data' function, then a wide class of problems can be formulated as

$$Lu = f. \tag{59}$$

The residual error is defined as the difference of each side of Equation (59):

$$r = Lu - f. \tag{60}$$

Roughly speaking, the FEM solution u_h is constructed such that

$$\int_\Omega (Lu_h - f)\phi_j \, d\Omega = 0. \tag{61}$$

Here, Ω represents the domain where (59) is to be satisfied, and ϕ_j are the weighting functions. There are at least two ways of interpreting the FEM solution that we call 'physical' and 'geometrical'. The physical interpretation says that the FEM solution is the particular finite-dimensional approximation that, for given boundary conditions, minimizes the stored energy in the problem. The geometrical interpretation says that the FEM solution is the projection of the exact solution to the finite-dimensional approximation space. Adopting the so-called Galerkin procedure to be described in the following section, the physical and geometrical solutions coincide.

FEM solution provides explicit control over the global error, contrary to the FDTD. Another characteristic distinction is that FEM is normally applied as a frequency domain method, i.e.

time-harmonic fields are assumed. There are hybrid methods that combine the geometric versatility of FEM and efficiency of time-domain algorithms [92], and they are potentially interesting alternatives in the future; nevertheless, hybrid methods are not considered in this work.

5.2 Trial and testing functions

We look for the FEM solution in a finite-dimensional subspace V_h of the infinite-dimensional function space V where the solution is assumed to be found, usually $V = \mathrm{H}^1$. For convenience, we choose a set of basis functions Φ_i such that

$$V_h = \mathrm{span}\{\Phi_i\}_{i=1}^{N} \ . \tag{62}$$

The approximation u_h is then expanded as a sum of the basis functions:

$$u_h = \sum_{i=1}^{N} c_i \Phi_i . \tag{63}$$

From the FEM point of view, there are two types of boundary conditions, essential and natural. The essential boundary conditions are implied in the choice of the basis, while the natural boundary conditions will be approximately satisfied during the solution without any special effort. Typically, essential boundary conditions are Dirichlet type (fixed boundary values), and natural boundary conditions are homogeneous Neumann type (zero normal derivative).

Inserting (63) into Equation (61), using the linearity of the operator L and arranging terms, we have

$$\sum_{i=1}^{N} c_i \int_{\Omega} (L\Phi_i)\phi_j \, d\Omega = \int_{\Omega} f\phi_j \, d\Omega . \tag{64}$$

In conventional terminology, functions Φ_i are called trial, approximating or expansion functions, and functions ϕ_j are called testing functions.

Although Equation (64) already provides a means to construct a set of linear equations for the solution of the expansion coefficients c_i, the form of the operator L often allows integration by parts (= application of Green's identities), resulting a symmetric bilinear form, which can be expressed symbolically as

$$\int_{\Omega} (L\Phi_i)\phi_j \, d\Omega = \ldots \text{integration by parts} \ldots = a(\Phi_i, \phi_j) = a(\phi_j, \Phi_i) . \tag{65}$$

So far, we have left the choice of ϕ_j open. Usually a satisfactory choice is to make the testing functions equal the trial functions: $\phi_j = \Phi_j$. This choice leads to a weak Galerkin solution of the original problem. The name "weak" comes from weaker assumptions made to the solution. Typically, strong solution of (59) belongs to H^2, but the weak solution is only assumed to belong to H^1, which is a larger space. The symmetry of the form $a(\cdot\,,\cdot)$ results in

symmetric coefficient matrix for the Galerkin solution, enabling special matrix decomposition techniques to be applied.

5.3 Choice of basis functions

There are no restrictions for the choice of basis functions Φ_i, apart from the linear independence, proper smoothness, and fulfillment of essential boundary conditions. Otherwise one may construct the basis as desired, compromising between simplicity and efficiency. For convenience and programmability, the basis should be easily generated and convergent, such that the approximation space V_h becomes eventually dense in V. Loosely speaking, any given point in V should be able to be approximated within any given accuracy by a linear combination of a finite number of basis functions.

The simplest and most traditional basis consists of piecewise linear functions. The degrees of freedom are simply the nodal values of the finite element mesh. This basis leads to very sparse element matrices and is therefore widely used, allowing problems with tens of thousands of unknowns to be solved in a moderate workstation. The accuracy is controlled solely by the mesh density. The associated method is often labeled as an *h*-version FEM.

A classical alternative to the *h*-version FEM is the *p*-version FEM [9], where the basis functions are piecewise polynomials, and the degree of the polynomials is taken as a parameter. The justification for the use of more complicated *p*-elements lies in the fact that the approximation properties improve *exponentially* with respect to the basis order, but only *algebraically* with respect to the mesh density: typically error is proportional to h^p, the actual formula depending on the error measure. *p*-elements lead to denser element matrices, because the basis functions are more overlapping. For a given number of degrees of freedom, *p*-elements require more storage and CPU-time for the solution, but on the other hand, the accuracy is usually considerably better. For a given level of accuracy, the required number of degrees of freedom is typically so much less that the total computational burden is in favor of *p*-elements. The accuracy is controlled by both the mesh density and the order of the basis.

p-elements allow very sparse meshing of the geometrical domain. This may be crucial in 3-D problems, where automatic mesh generation is considerably more difficult than in 2-D. In order to fully exploit large elements, one must be able to treat curved boundaries accurately. This is discussed further in Section 5.5.

There are several possibilities for constructing high-order bases. A classical construction [9] is a high-order interpolating basis: a set of additional nodes is introduced in the element, and to each such node there corresponds one basis function. The basis function attains value 1 at one node and 0 at all other nodes. Figure 14 depicts a six-node 2^{nd}-order element, and one of the local basis functions. The values at the nodes specify completely the form of the approximation, and thus, the nodal values are also the degrees of freedom.

There are at least two shortcomings in the interpolating basis. First, a basis of order *p* is completely different from the basis of order *p*-1, which makes the convergence analysis expensive, because each order has a separate set of basis functions. Second, it is difficult to join two elements of different orders. An early proposition to allow variable-order elements is given in [93].

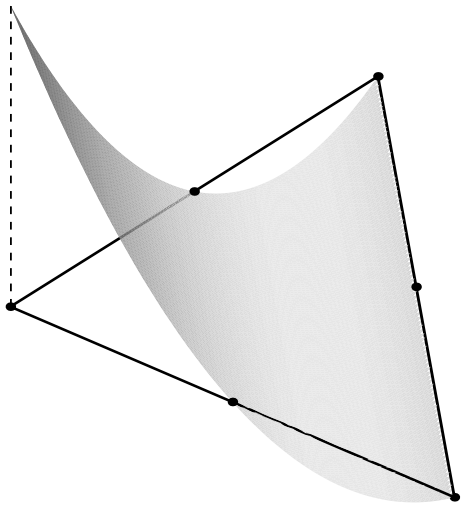

Figure 14. Second-order six-node element and the local basis function associated to one of the vertex nodes.

In so-called hierarchic basis [94], the local basis functions for 2-D elements are divided into three categories: 1) vertex modes, 2) edge modes and 3) inner modes. For a p^{th}-order basis, they are grouped as follows:

- one linear basis function associated to each vertex. Vertex modes attain value 1 at one vertex and vanish at the other vertices.
- one basis function of each degree 2…p associated to each edge. Edge modes attain polynomial form at one edge and vanish at other edges.
- q-2 inner basis functions of each degree q = 3…p. The inner modes vanish on all edges.

Thus, there are (p+1)(p+2)/2 basis functions altogether spanning a complete 2-variable polynomial of degree p. In the construction, Lagrange polynomials are used, providing some level of orthogonality between the basis functions, and consequently, stable numerical properties. Hierarchy means that a basis of order p-1 is a subset of the basis of order p. A single integration provides system matrices for all orders up to p, simplifying considerably the convergence analysis along increased order of the basis.

Varying the order of the individual elements over the mesh is also a simple matter. The common degrees of freedom of two adjacent elements are the coefficients of the vertex and edge modes associated to the common vertices and edge. Suppose we wish to have element of order eight on the right and of order four on the left. To make the two elements compatible, we can simply supply the 4^{th}-order basis on the left by the 5^{th}-, 6^{th}-, 7^{th}- and 8^{th}-order edge modes. Now, the approximation space on the left is not purely 4^{th}-order but a bit larger, while the space on the right is completely 8^{th}-order. The variable-order mesh can be used easily and efficiently, if one can justifiably assume slow variations of the field in some regions of the problem, allowing the use of low-order elements in those regions [P6].

Due to the above advantages, especially the clear organization and possibility for simple realization of variable-order mesh, we used exclusively the hierarchic basis in all the studies reported in [P6].

5.4 Field singularities

It is well known that sharp re-entrant corners result in local field singularities to the electromagnetic field [95-99]. If the corner geometry is regular enough, the form of the singularity is known. For example, if the corner is an infinite perfectly conducting wedge with angle α, then the longitudinal field components behave as r^{ν} close to the wedge tip, where $\nu = \pi/(2\pi-\alpha)$. Always $\nu \geq 1/2$. The transverse components are one order more singular, behaving as $r^{\nu-1}$.

The singularity problem in FEM point of view has been discussed previously in [100-105] for scalar elements and [106-108], for vector elements. Singularity is also treated in some length in the textbook [84]. In paper [P6], an error estimate for eigenvalues of the scalar Helmholtz equation is derived: the relative error of the eigenvalues is bounded by the sum of relative errors of the corresponding field distributions in H^1-seminorm and L_2-norm. Since the latter is typically much smaller, the relevant measure for the accuracy of the eigenvalues (= cut-off frequencies) is the H^1- error.

In the most singular case, the solution is of the order $r^{1/2}$, corresponding to zero-angle wedge in e.g. idealized model of fin lines or microstrip lines. If the approximation is a polynomial, then the gradient of the difference between exact and approximate solutions is unbounded. Therefore, it is obvious that the immediate neighborhood of the singular point contributes significantly to the H^1-error, resulting high error bound to the computed eigenvalues.

Let us mention, that although we can formally write the Helmholtz equation also to the *transverse* field in a singular problem, the transverse field does not belong to the space H^1. This implies that the usual weak formulation of the Helmholtz equation for the transverse components is not valid – we could in principle obtain a convergent sequence of approximations, but each approximation belongs to H^1, and so does their limit, because H^1 is a complete space [83]. In other words, even if we happened to obtain a convergent sequence of approximations, the limit would be incorrect, because the true solution is not in H^1. This example highlights the importance of the concept of smoothness of the solution and proper formulation of a problem.

In paper [P6] we supply the polynomial basis by an additional function, especially constructed to have the correct singular form. Now, this singular basis function serves to 'catch' the most rapidly changing part of the field close to the singularity. What is not caught by the singular function is the smooth part of the field, which is easily caught by the polynomial part of the basis. Convergence analysis and comparison with other published results suggest that our approach with hierarchic *p*-elements is comparable or superior to previous studies in terms of degrees of freedom required to reach a certain error level. Also, there seems to be novel aspects in relating the H^1-error of the solution and the accuracy of the computed eigenvalue.

5.5 Curved boundaries

Classical construction of FEM solution assumes that the boundary of the problem is polygonal, i.e. the entire domain can be subdivided into a finite number of triangles. If, however, the boundary contains curved parts, one has several options. The simplest option is

to approximate the curved boundary by a polygon. This is an adequate choice for low-order elements. Another classical option is to use polynomial approximation of the boundary geometry. Quite often, the basis functions themselves are also used as mapping functions: if the basis is a 2^{nd}-order one, then curved parts of the boundary are approximated by 2^{nd}-order polynomial curves. This approach leads to so-called isoparametric elements [84]. Third option is to use the so-called blending function method to *exactly* describe an arbitrary curved boundary geometry [109-111]. This option is especially efficient if combined with high-order basis [94].

In [112], Kärkkäinen utilizes the blending function method to a number of cases having curved boundaries. Hierarchic high-order basis is combined with singular basis function [P6] where necessary. A circular fin line serves as a singular reference problem having a known analytical solution. The results clearly demonstrate that to obtain high accuracy and to avoid large number of elements, it is advisable to use the blending function method. An exponential convergence of the computed cut-off frequency with respect to degrees of freedom is obtained. The results of [112] provide further verification of the use of the singular basis functions, because the examples treated in [P6] lack analytical reference solutions.

6 Summary of publications

Paper **[P1]** describes a simple way to reduce numerical dispersion in the FDTD method. The starting point is the observation that the numerical dispersion resembles anisotropy. Would it be possible, then, to define the model medium as intentionally anisotropic in such a way that these anisotropies somehow cancel each other? The answer is *yes*, and the compensation possibility is revealed through careful examination of the numerical dispersion relation of anisotropic medium in FDTD. The compensation is realized through diagonal permittivity and permeability tensors, and there is no increase in CPU-time and memory requirements of the compensation. The compensation parameters are easily found for given grid resolution, cell shape and Courant-number. The main deficiency of the method is its frequency-dependence. It is demonstrated, however, that a considerable improvement can be achieved for a reasonable band by optimizing the reduction parameters at the low end of the band. Several examples in 2-D and 3-D are given to validate the compensation efficiency, involving both homogeneous and inhomogeneous problems. For highly non-cubical cells, a typical improvement in the accuracy is seen to be approximately equivalent to doubling the grid density.

Paper **[P2]** deals with a recently proposed absorbing boundary condition called perfectly matched layer (PML) [23]. A closed-form expression is given for the realized performance of PML in 1-D FDTD algorithm for propagating plane waves. It is confirmed that the simple 1-D formula can be used also to predict the reflection in 2-D simulations, and it seems probable that similar possibility exists also for 3-D problems. The analysis reveals that PML can be designed to absorb *perfectly* plane waves at discrete frequencies. It was not recognized before that zero reflection is possible for finite thickness PML. The formula is tested with a number of simulation experiments, and also some previously published simulation results [65] are reproduced using the closed-form expression. A novel design process for optimal conductivity profile in PML is outlined; the user is allowed to choose M independent (frequency,angle)-pairs for an M-layer PML such that the corresponding plane waves are perfectly absorbed. The application of the theory is demonstrated by a parallel-plate waveguide example, where in a four-layer PML, an improvement of 28 dB over a wide frequency band is gained, as compared to a traditional PML having the same thickness.

To achieve really optimal use of PML, the applicability of the reflection coefficient in 3-D should be verified, and the theory should be extended to evanescent waves.

Paper **[P3]** is an application of FDTD to a small-sized wide-band dielectric resonator antenna (DRA). The novelty in the algorithmic point of view is the improved coaxial probe model applied in the FDTD simulations. The improvement allows releasing the condition $\Delta x = \Delta y$ that was assumed in the previously published model. From the engineering point of view, the capabilities of FDTD have been used to gain physical insight to the complicated resonance phenomena taking place in the DRA structures. In addition, a sensitivity analysis has been carried out using FDTD to determine the critical prototype and simulation parameters (accuracy of dimensions, numerical dispersion, air gaps in different locations, losses etc.). Summarizing, we have showed that FDTD is very well suited for DRA analysis, and provided a generalized coaxial probe model to be used in any relevant simulations.

In paper **[P4]**, the properties of the so-called resistive voltage source (RVS) are discussed. RVS is commonly used in FDTD simulations as an excitation model of coaxial probes or dipole antennas. In the RVS formalism, the intended source impedance is given as a

parameter. The actually modeled source impedance is known to be distorted due to the cell capacitance [21]. In [P4], examples are given demonstrating that the distortion may be significant, thus affecting the S_{11}-parameter evaluation. To make the parameter evaluation insensitive to the distortion, we recommend evaluating only the input impedance, the simulation of which is confirmed to be independent of source cell capacitance. Furthermore, contrary to the preconception, the input impedance is seen to be independent on cell height as well, provided that the feed point is properly transformed to a suitable reference location, e.g. to the ground plane.

Paper **[P5]** presents a corrected thin-wire model in 2-D FDTD. It is shown that the traditional thin-wire model mixes rotational symmetry and Cartesian grid inconsistently, resulting in e.g. incorrect induced current in the wire. A simple modification to the thin-wire FDTD update equations is provided. Several tests are performed to investigate the new model. The results are convincing, demonstrating that the traditional thin-wire model simulates actually a significantly larger wire radius, while all tests performed with the new model indicate that the wire radius is correctly simulated.

The implications of paper [P5] may be far-reaching, since thin-wire structures are very common. After proper extension to 3-D, FDTD simulations involving e.g. coupling probes or wire antennas are expected to gain more accuracy. The improvement is expected to be especially high with very thin wires (wire radius of the order of 0.001λ or less).

Paper **[P6]** deals with the use of finite element method (FEM) in the analysis of waveguide structures containing concave singularities, e.g. fin lines. Only scalar bases are considered in this work. Error analysis of the cut-off wavenumber shows that the accuracy is bounded by the H^1-error of the field solution. This is important, because the conventional polynomial bases approximate singular fields poorly in H^1-norm. Therefore, a solution that might look physical and essentially correct (L_2-error of the order of 1 %) may have significant H^1-error (of the order of 10 %). Because the scalar solution represents a longitudinal component of the field, other field components are obtained by differentiation. Obviously differentiation of a polynomial solution cannot give correctly the unbounded transverse components in the neighborhood of the singularity. To overcome these shortcomings, inclusion of a novel, locally supported singular basis function is proposed. Several examples are considered, and the results are compared with previously published works. In this context, the hierarchic *p*-version elements have proven to be advantageous, allowing variable-order mesh to be realized.

7 Conclusions

In this thesis, we have considered a number of topical themes related to numerical methods in radio engineering. Most of the work concentrates on algorithm developments for the finite-difference time-domain method, while a secondary part is devoted to the finite element method. The results of the thesis work are published in refereed international journals and conferences, and they are hoped to serve general use.

The novel scientific contents of the thesis are the following, ordered according to the author's personal opinion in decreasing order of importance:

- [P2] Closed-form reflection coefficient for the discretized PML. Observation and demonstration that a finite-thickness PML in FDTD can be designed to absorb plane waves with zero reflection. Description of an efficient optimization procedure for the conductivity profile. Demonstration that optimization can yield orders of magnitude improvement of the reflection coefficient in a wide frequency band, when compared to classical PML of same thickness.
- [P5] Correction of the thin-wire equations in FDTD. Verification of the accuracy of the corrected model by direct evaluation of the effective radius, and indirectly by consistency tests.
- [P6] Derivation of a simple error estimate in FEM for the cut-off frequencies of a homogeneous waveguide in terms of field solution errors. Proposition of a novel singular basis function. Comparative experiments with variable-order meshes.
- [P1] Development of a novel numerical dispersion reduction scheme for FDTD through anisotropy compensation. Recognition of prominent dependence of numerical dispersion on cell shape.
- [P4] Demonstration that the simulated input impedance of an antenna does not depend on source cell height in the resistive voltage source model, if the reference point is properly moved to a common reference plane. Justification that the apparent discrepancies observable in monopole antenna simulations result from different modeling of field singularity on top of the monopole.
- [P3] Development of a generalized coaxial probe model for FDTD simulations.

The order is of course disputable, and would be different, if the criterion were e.g. practical applicability. In that case, the order could be [P5], [P4], [P3], [P2], [P1], [P6].

In the author's view, the following are examples of interesting themes that deserve further development in the future:

- Effective modeling of inhomogeneous materials in pseudospectral time-domain (PSTD) method and in high-order FDTD.
- Development of efficient FDTD algorithms to model thin multilayer printed circuit boards, applying 2-D FDTD between the layers.
- Further examination of the field singularity problem in FDTD, aiming at better accuracy in microstrip structures, patch antennas etc.
- Further development and application of lumped elements in FDTD, especially active and nonlinear components.
- Examination of time-domain FEM algorithms.
- Development of singular basis functions for 3-D vector finite elements.
- Development of singular basis functions for the method of moments.

Appendix

Matlab-code "**comp3d**" finds anisotropy parameters (ε_x, ε_y, ε_z) that compensate numerical dispersion in a 3-D FDTD grid. Input parameters are: Courant-number Q_3, cell shape parameters $Z_y = \Delta x/\Delta y$, $Z_z = \Delta x/\Delta z$, and resolution parameter $R = \lambda / \sqrt{\Delta x^2 + \Delta y^2 + \Delta z^2}$.

```
function [ex,ey,ez]=comp3d(Q3,Zy,Zz,R);
% Jaakko Juntunen 21.11.2000

Amax = pi/(3*R*asin(sin(pi/(R*sqrt(3)))/sqrt(3))); E = (Amax - 1)/2;
K1 = pi/(R*sqrt(1+1/Zy^2+1/Zz^2));
a = sin(K1/(1-E))^2/(Zy^2*sin(K1/((1-E)*Zy))^2);
b = sin(K1/(1-E))^2/(Zz^2*sin(K1/((1-E)*Zz))^2);
K2 = sqrt(1+a*Zy^2+b*Zz^2);
ex = K2/(K1*Q3*sqrt(a*b))*asin(Q3*sin(K1/(1-E))/K2); ey = a*ex; ez = b*ex;
```

Matlab-code "**rho_1d**" evaluates the reflection coefficient from 1-D PML. Input parameters are: Courant-number Q, resolution parameter $R = \lambda/\Delta x$, and normalized conductivity values σ^N. R can be given as vector.

```
function rho = rho_1d(Q,R,s);
% Jaakko Juntunen 21.11.2000

N = length(s); W = 2/Q*sin(pi*Q./R); k_delta = 2*asin(W/2);
for i = 1:N, T(i,:) = j*W + s(i)*cos(pi*Q./R); end;
CUM = zeros(size(R));
for i = 1:N, CUM = CUM + T(N+1-i,:); CUM = 1./CUM; end;
U = (j*W + CUM).*exp(j*k_delta/2);
rho = (U - exp(j*k_delta))./(1 + U);
```

Matlab-code "**rho_2d_exact**" evaluates the reflection coefficient from 2-D PML. Input parameters are: angle of incidence α, $Z = \Delta x/\Delta y$, Courant-number Q_2, resolution parameter $R_2 = \lambda / \sqrt{\Delta x^2 + \Delta y^2}$, and normalized conductivity values σ^N. Either α or R_2 can be given as vector. "rho_2d_exact" calls function "disper", given below.

```
function rho = rho_2d_exact(alpha,Z,Q2,R2,s);
% Jaakko Juntunen 21.11.2000

v = disper(alpha,Z,Q2,R2); r = pi./(v.*R2*sqrt(1 + Z^2));
kxdx2 = Z*r.*cos(alpha); kydy2 = r.*sin(alpha);
W1 = pi*Q2*Z./(R2*(1 + Z^2)); W = 2*sqrt(1 + Z^2)*sin(W1)/Q2;
P = 4*Z^2*sin(kydy2).^2./W.^2;
ss = size(s); [Ls,b] = max(ss); if b==2, s = s'; end;
if 2*floor(Ls/2)==Ls, s=[0;s]; Ls = Ls + 1; end;  % let length(s) be odd

for i = 1:Ls,
   S(i,:) = s(i)*cos(W1);
   if 2*floor(i/2)==i,
      T(i,:) = S(i,:) + j*W;
   else
      T(i,:) = (S(i,:) + j*W).*(1 - P);
   end;
end;
```

```
CUM = 0; for i = 1:Ls, CUM = CUM + T(Ls + 1 - i,:); CUM = 1./CUM; end;
U = 2./W.*sin(kxdx2).*exp(j*kxdx2).*(j*W + CUM);
rho = (exp(j*2*kxdx2) - U)./(1 + U);
```

Function "**disper**" evaluates numerical dispersion in the 2-D FDTD grid using Newton iteration. This function is called from "rho_2d_exact".

```
function v = disper(alpha,Z,Q2,R2);
% Jaakko Juntunen 21.11.2000

for i = 1:length(R2),
   R = R2(i);
   c1 = (1 + Z^2)/(Q2^2*Z^2)*sin(pi*Q2*Z/(R*(1+Z^2)))^2;
   tol = pi/(R*sqrt(1 + Z^2))*1e-10;
   r_old = pi/(R*sqrt(1 + Z^2))*ones(size(alpha)); err = 2*tol;
   while err>tol,
      f = sin(r_old.*sin(alpha)).^2 + sin(Z*r_old.*cos(alpha)).^2/Z^2 - c1;
      df = cos(alpha).*sin(2*Z*r_old.*cos(alpha))/Z + ...
         sin(alpha).*sin(2*r_old.*sin(alpha));
      r_new = r_old - f./df; err = max(abs(r_new - r_old)); r_old = r_new;
   end;
   v(:,i) = pi./(R*sqrt(1 + Z^2).*r_old);
end;
```

The operation of the Matlab-code "**rho_2d**" is equivalent to "rho_2d_exact", except that only R_2 can be given as vector. "rho_2d" calls function "rho_1d", given above.

```
function rho = rho_2d(alpha,Z,Q2,R2,s);
%  Jaakko Juntunen 21.11.2000
Q1 = Q2/(cos(alpha)*sqrt(1+Z^2));
R1 = R2*sqrt(1+Z^2)/(Z*cos(alpha));
rho = rho_1d(Q1,R1,cos(alpha)*s);
```

References

[O1] Zhao, A. P., Juntunen, J. S., Räisänen, A. V.: Generalized material independent PML absorbers for the FDTD simulation of electromagnetic waves in arbitrary anisotropic dielectric and magnetic media. *IEEE Microwave and Guided Wave Letters*, Vol. 8, No. 2, 1998, pp. 52-54.

[O2] Zhao, A. P., Juntunen, J. S., Räisänen, A. V.: Relationship between the compact complex and real variable 2-D FDTD methods in arbitrary anisotropic dielectric waveguides. *IEEE MTT-S International Microwave Symposium Digest*, Denver, 1997, pp. 83-87.

[O3] Zhao, A. P., Juntunen, J. S., Räisänen, A. V.: A generalized compact 2-D FDTD model for the analysis of guided modes of anisotropic waveguides with arbitrary tensor permittivity. *Microwave and Optical Technology Letters*, Vol. 18, No. 1, 1998, pp. 17-23.

[O4] Zhao, A. P., Juntunen, J. S., Räisänen, A. V.: An efficient FDTD algorithm for the analysis of microstrip patch antennas printed on a general anisotropic dielectric substrate. *IEEE Transactions on Microwave Theory and Techniques*, Vol. 47, No. 7, 1999, pp. 1142-1146.

[O5] Juntunen, J. S., Tsiboukis, T. D.: On the FEM treatment of wedge singularities in waveguide problems. *IEEE AP-S International Symposium Digest*, Orlando, 1999, pp. 464-467.

[O6] Juntunen, J. S.: Curved high-order finite elements for numerical solution of the Helmholtz equation in complicated geometries. *Proceedings of the 4th International Conference on Unconventional Electromechanical and Electrical Systems (UEES'99)*, St. Petersburg, 1999, pp. 867-872.

[O7] Juntunen, J. S., Zhao, A. P.: Auto-extraction of the correct field distribution of guided modes from 2-D FDTD simulation. *URSI/IEEE/IRC XXI National Convention on Radio Science*, Espoo, 1996, pp. 135-136.

[1] Waldschmidt, G., Taflove, A.: The determination of the effective radius of a filamentary source in the FDTD mesh. *IEEE Microwave and Guided Wave Letters*, Vol. 10, No. 6, 2000, pp. 217-219.

[2] Piket-May, M., Taflove, A., Baron, J.: FD-TD modeling of digital signal propagation in 3-D circuits with passive and active loads. *IEEE Transactions on Microwave Theory and Techniques*, Vol. 42, No. 8, 1994, pp. 1514-1523.

[3] Li, B.-J., Liu, P.-L.: Analysis of far-field patterns of microdisk resonators by the finite-difference time-domain method. *IEEE Journal of Quantum Electronics*, Vol. 33, No. 9, 1997, pp. 1489-1491.

[4] McKown, J. W., Hamilton, R. L.: Ray tracing as a design tool for radio networks. *IEEE Network Magazine*, Vol. 5, No. 6, 1991, pp. 27-30.

[5] Pantić, Z., Mittra, R.: Quasi-TEM analysis of microwave transmission lines by the finite-element method. *IEEE Transactions on Microwave Theory and Techniques*, Vol. MTT-34, No. 11, 1986, pp. 1096-1103.

[6] Salazar-Palma, M., Ferragut, L., Mustieles, F.-J., Hernández-Gil, F.: Assessing the error of transmission-line quasi-static analyses by means of a mixed finite element method. *IEEE AP-S International Symposium Digest*, Ontario, 1991, pp. 1232-1235.

[7] Carson, C. T., Combrell, G. K.: Upper and lower bounds on the characteristic impedance impedance of TEM mode transmission lines. *IEEE Transactions on Microwave Theory and Techniques*, Vol. MTT-14, No. 10, 1966, pp. 497-498.

[8] Taflove, A. (editor): *Advances in Computational Electrodynamics: The Finite-Difference Time-Domain Method*, Artech House, Norwood, MA, 1998, 724 p.

[9] Zienkiewicz, O. C.: *The Finite Element Method*. 3rd expanded and revised ed., McGraw-Hill, London, 1977, 787 p.

[10] Yee, K. S.: Numerical solution of initial boundary value problems involving Maxwell's equations in isotropic media. *IEEE Transactions on Antennas and Propagation*, Vol. AP-14, No. 3, 1966, pp. 302-307.

[11] Taflove, A., Brodwin, M. E.: Numerical solution of steady-state electromagnetic scattering problems using the time-dependent Maxwell's equations. *IEEE Transactions on Microwave Theory and Techniques*, Vol. MTT-23, No. 8, 1975, pp. 623-630.

[12] Celuch-Marcysiak, M., Gwarek, W.K.: On the nature of solutions produced by finite difference schemes in time domain, invited paper, *International Journal of Numerical Modelling – Electronic Networks, Devices and Fields*, Vol. 12, No. 1/2, 1999, pp. 23-40.

[13] Kunz, K. S., Luebbers, R. J.: *The Finite Difference Time Domain Method for Electromagnetics*, CRC Press, Boca Raton, FL, 1993, 448 p.

[14] Zhao, A. P., Räisänen, A. V., Cvetkovic, S. R.: A fast and efficient FDTD algorithm for the analysis of planar microstrip discontinuities by using a simple source excitation scheme. *IEEE Microwave and Guided Wave Letters*, Vol. 5, No. 10, 1995, pp. 341-343.

[15] Mroczkowski, C., Gwarek, W. K.: Microwave circuits described by two-dimensional vector wave equation and their analysis by FD-TD method, *Proceedings of 21st European Microwave Conference*, Stuttgart, 1991, pp. 199-204.

[16] Asi, A., Shafai, L.: Dispersion analysis of anisotropic inhomogeneous waveguides using compact 2D-FDTD. *IEE Electronics Letters*, Vol. 28, No. 15, 1992, pp. 1451-1452.

[17] Xiao, S., Vahldieck, R., Jin, H.: Full-wave analysis of guided wave structures using a novel 2-D FDTD. *IEEE Microwave and Guided Wave Letters*, Vol. 2, No. 5, 1992, pp. 165-167.

[18] Tirkas, P. A., Balanis, C. A.: Finite-difference time-domain method for antenna radiation. *IEEE Transactions on Antennas and Propagation*, Vol. 40, No. 3, 1992, pp. 334-340.

[19] Maloney, J. G., Shlager, K. L., Smith, G. S.: A simple FDTD model for transient excitation of antennas by transmission lines. *IEEE Transactions on Antennas and Propagation*, Vol. 42, No. 2, 1994, pp. 289-292.

[20] Sui, W., Christensen, D. A., Durney, C. H.: Extending the two-dimensional FDTD method to hybrid electromagnetic systems with active and passive lumped elements. *IEEE Transactions on Microwave Theory and Techniques*, Vol. 40, No. 4, 1992, pp. 724-730.

[21] Pekonen, O. P. M., Xu, J., Nikoskinen, K. I.: Rigorous analysis of circuit parameter extraction from an FDTD simulation excited with a resistive voltage source. *Microwave and Optical Technology Letters*, Vol. 12, No. 4, 1996, pp. 205-210.

[22] Mur, G.: Absorbing boundary conditions for the finite-difference approximation of the time-domain electromagnetic-field equations. *IEEE Transactions on Electromagnetic Compatibility*, Vol. EMC-23, No. 4, 1981, pp. 377-382.

[23] Bérenger, J.-P.: A perfectly matched layer for the absorption of electromagnetic waves. *Journal of Computational Physics*, Vol. 114, 1994, pp. 185-200.

[24] Zhang, X., Mei, K. K.: Time-domain finite difference approach to the calculation of the frequency-dependent characteristics of microstrip discontinuities. *IEEE Transactions on Microwave Theory and Techniques*, Vol. 36, No. 12, 1988, pp. 1775-1787.

[25] Przybyszewski, P., Mrozowski, M.: A conductive wedge in Yee's mesh. *IEEE Microwave and Guided Wave Letters*, Vol. 8, No. 2, 1998, pp. 66-68.

[26] Harms, P. H., Lee, J.-F., Mittra, R.: A study of the nonorthogonal FDTD method versus the conventional FDTD technique for computing resonant frequencies of cylindrical cavities. *IEEE Transactions on Microwave Theory and Techniques*, Vol. 40, No. 4, 1992, pp. 741-746.

[27] Gwarek, W. K.: Analysis of an arbitrarily-shaped planar circuit – a time-domain approach. *IEEE Transactions on Microwave Theory and Techniques*, Vol. MTT-33, No. 10, 1985, pp. 1067-1072.

[28] Railton, C. J., Schneider, J. B.: An analytical and numerical analysis of several locally conformal FDTD schemes. *IEEE Transactions on Microwave Theory and Techniques*, Vol. 47, No. 1, 1999, pp. 56-66.

[29] Mur, G.: The modeling of singularities in the finite-difference approximation of the time-domain electromagnetic-field equations. *IEEE Transactions on Microwave Theory and Techniques*, Vol. MTT-29, No. 10, 1981, pp. 1073-1077.

[30] Fang, J.: *Time domain finite difference computation for Maxwell's equations*, Ph.D. dissertation, Univ. California, Berkeley, CA, 1989, 174 p.

[31] Deveze, T., Beaulieu, L., Tabbara, W.: A fourth order scheme for the FDTD algorithm applied to Maxwell's equations. *IEEE AP-S International Symposium Digest*, Chicago, 1992, pp. 346-349.

[32] Turkel, E., Yefet, A.: Fourth order method for Maxwell equations on a staggered mesh. *IEEE AP-S International Symposium Digest*, Montreal, 1997, pp. 2156-2159.

[33] Young, J. L., Gaitonde, D., Shang, J. J. S.: Toward the construction of a fourth-order difference scheme for transient EM wave simulation: staggered grid approach. *IEEE Transactions on Antennas and Propagation*, Vol. 45, No. 11, 1997, pp. 1573-1580.

[34] Gustafsson, B., Kreiss, H.-O., Oliger, J.: *Time Dependent Problems and Difference Methods*, Wiley-Interscience, New York, NY, 1996, 656 p.

[35] Haussmann, G., Piket-May, M.: Modeling interface discontinuities and boundary conditions for a dispersion-optimized finite-difference time-domain method. *IEEE AP-S International Symposium Digest*, Atlanta, 1998, pp. 1820-1823.

[36] Shlager, K. L., Schneider, J. B.: Relative accuracy of several low-dispersion finite-difference time-domain schemes. *IEEE AP-S International Symposium Digest*, Orlando, 1999, pp. 168-171.

[37] Krumpholz, M., Katehi, L. P. B.: MRTD: new time-domain schemes based on multiresolution analysis. *IEEE Transactions on Microwave Theory and Techniques*, Vol. 44, No. 4, 1996, pp. 555-571.

[38] Hadi, M. F., Piket-May, M.: A modified FDTD (2,4) scheme for modeling electrically large structures with high-phase accuracy. *IEEE Transactions on Microwave Theory and Techniques*, Vol. 45, No. 2, 1997, pp. 254-264.

[39] Cole, J. B.: A high-accuracy realization of the Yee algorithm using non-standard finite differences. *IEEE Transactions on Microwave Theory and Techniques*, Vol. 45, No. 6, 1997, pp. 991-996.

[40] Forgy, E. A., Chew, W. C.: An efficient FDTD algorithm with isotropic numerical dispersion on an overlapped lattice. *IEEE AP-S International Symposium Digest*, Atlanta, 1998, pp. 1812-1815.

[41] Nehrbass, J. W., Jevtić, J. O., Lee, R.: Reducing the phase error for finite-difference methods without increasing the order. *IEEE Transactions on Antennas and Propagation*, Vol. 46, No. 8, 1998, pp. 1194-1201.

[42] Forgy, E. A., Chew, W. C.: A new FDTD formulation with reduced dispersion for the simulation of wave propagation through inhomogeneous media. *IEEE AP-S International Symposium Digest*, Orlando, 1999, pp. 1316-1319.

[43] Liu, Q. H.: The PSTD algorithm: A time-domain method requiring only two cells per wavelength. *Microwave and Optical Technology Letters*, Vol. 15, No. 3, 1997, pp. 158-165.

[44] Lindell, I.: *Radioaaltojen eteneminen*, (in Finnish) Otatieto Oy, Helsinki, 1996, 262 p.

[45] Taflove, A.: *Computational Electrodynamics. The Finite-Difference Time-Domain Method*, Artech House Inc., Norwood, MA, 1995, 599 p.

[46] Bayliss, A., Turkel, E.: Radiation boundary conditions for wave-like equations, *Communications on Pure and Applied Mathematics*, Vol. 23, 1980, pp. 707-725.

[47] Engquist, B., Majda, A.: Absorbing boundary conditions for the numerical simulation of waves. *Mathematics of Computation*, Vol. 31, 1977, pp. 629-651.

[48] Trefethen, L. N., Halpern, L.: Well-posedness of one-way wave equations and absorbing boundary conditions. *Mathematics of Computation*, Vol. 47, 1986, pp. 421-435.

[49] Higdon, R. L.: Numerical absorbing boundary conditions for the wave equation. *Mathematics of Computation*, Vol. 49, 1987, pp. 65-90.

[50] Liao, Z. P., Wong, H. L., Yang, B. P., Yuan, Y. F.: A transmitting boundary for transient wave analyses. *Scientia Sinica* (series A), vol. XXVII, 1984, pp. 1063-1076.

[51] Mei, K. K., Fang, J.: Superabsorption – a method to improve absorbing boundary conditions. *IEEE Transactions on Antennas and Propagation*, Vol. 40, No. 9, 1992, pp. 1001-1010.

[52] Katz, D. S., Thiele, E. T., Taflove, A.: Validation and extension to three dimensions of the Berenger PML absorbing boundary condition for FD-TD meshes. *IEEE Microwave and Guided Wave Letters*, Vol. 4, No. 8, 1994, pp. 268-270.

[53] Chew, W. C., Weedon, W. H.: A 3D perfectly matched medium from modified Maxwell's equations with stretched coordinates. *Microwave and Optical Technology Letters*, Vol. 7, No. 13, 1994, pp. 599-604.

[54] Rappaport, C. M.: Perfectly matched absorbing boundary conditions based on anisotropic lossy mapping of space. *IEEE Microwave and Guided Wave Letters*, Vol. 5, No. 3, 1995, pp. 90-92.

[55] Sacks, Z. S., Kingsland, D. M., Lee, R., Lee, J. F.: A perfectly matched anisotropic absorber for use as an absorbing boundary condition. *IEEE Transactions on Antennas and Propagation*, Vol. 43, No. 12, 1995, pp. 1460-1463.

[56] Zhao, L., Cangellaris, A. C.: GT-PML: Generalized theory of perfectly matched layers and its application to the reflectionless truncation of finite-difference time-domain grids. *IEEE Transactions on Microwave Theory and Techniques*, Vol. 44, No. 12, 1996, pp. 2555-2563.

[57] Berenger, J.-P.: Perfectly matched layer for the FDTD solution of wave-structure interaction problems. *IEEE Transactions on Antennas and Propagation*, Vol. 44, No. 1, 1996, pp. 110-117.

[58] Fang, J., Wu, Z.: Closed-form expression of numerical reflection coefficient at PML interfaces and optimization of PML performance. *IEEE Microwave and Guided Wave Letters*, Vol. 6, No. 9, 1996, pp. 332-334.

[59] Lazzi, G., Gandhi, O. P.: On the optimal design of the PML absorbing boundary condition for the FDTD code. *IEEE Transactions on Antennas and Propagation*, Vol. 45, No. 5, 1997, pp. 914-916.

[60] Zhao, L., Cangellaris, A. C.: The generalized theory of perfectly matched layers (GT-PML): numerical reflection analysis and optimization. *IEEE AP-S International Symposium Digest*, Montreal, 1997, pp. 1896-1899.

[61] Marengo, E. A., Rappaport, C. M., Miller, E. L.: Optimum PML ABC conductivity profile in FDTD. *IEEE Transactions on Magnetics*, Vol. 35, No. 5, 1999, pp. 1506-1509.

[62] Wu, Z., Fang, J.: Numerical implementation and performance of perfectly matched layer boundary condition for waveguide structures. *IEEE Transactions on Microwave Theory and Techniques*, Vol. 43, No. 12, 1995, pp. 2676-2683.

[63] Berenger, J.-P.: Improved PML for the FDTD solution of wave-structure interaction problems. *IEEE Transactions on Antennas and Propagation*, Vol. 45, No. 3, 1997, pp. 466-473.

[64] Moerloose, J. D., Stuchly, M. A.: Reflection analysis of PML ABC's for low-frequency applications. *IEEE Microwave and Guided Wave Letters*, Vol. 6, No. 4, 1996, pp. 177-179.

[65] Winton, S. C., Rappaport, C. M.: Specifying PML conductivities by considering numerical reflection dependencies. *IEEE Transactions on Antennas and Propagation*, Vol. 48, No. 7, 2000, pp. 1055-1063.

[66] Bazaraa, M. S., Sherali, H. D., Shetty, C. M.: *Nonlinear Programming*, John Wiley & Sons, Inc., New York, NY, 1993, 638 p.

[67] Fang, J., Wu, Z.: Generalized perfectly matched layer for the absorption of propagating and evanescent waves in lossless and lossy media. *IEEE Transactions on Microwave Theory and Techniques*, Vol. 44, No. 12, 1996, pp. 2216-2222.

[68] Umashankar, K. R., Taflove, A.: A novel method to analyze electromagnetic scattering of complex objects. *IEEE Transactions on Electromagnetic Compatibility*, Vol. EMC-24, No. 4, 1982, pp. 397-405.

[69] Ramahi, O. M.: The complementary operators method in FDTD simulations. *IEEE Antennas and Propagation Magazine*, Vol. 39, No. 6, 1997, pp. 33-45.

[70] Ramahi, O. M., Schneider, J. B.: Comparative study of the PML and C-COM mesh-truncation techniques. *IEEE Microwave and Guided Wave Letters*, Vol. 8, No. 2, 1998, pp. 55-57.

[71] Pozar, D. M.: *Microwave Engineering.* Addison-Wesley, Reading, MA, 1990, 726 p.

[72] Izadian, J. S., Izadian, S. M.: *Microwave transition design*. Artech House, London, 1988, 150 p.

[73] Tam, M. K., Murch, R. D.: Half volume dielectric resonator antenna designs. *IEE Electronics Letters*, Vol. 33, No. 23, 1997, pp. 1914-1916.

[74] Lehmus, O., Ollikainen, J., Vainikainen, P.: Characteristics of half-volume DRAs with different permittivities. *IEEE AP-S International Symposium Digest*, Orlando, 1999, pp. 22-25.

[75] Umashankar, K. R., Taflove, A., Beker, B.: Calculation and experimental validation of induced currents on coupled wires in an arbitrary shaped cavity. *IEEE Transactions on Antennas and Propagation*, Vol. AP-35, No. 11, 1987, pp. 1248-1257.

[76] Taflove, A., Umashankar, K. R., Beker, B., Harfoush, F., Yee, K. S.: Detailed FD-TD analysis of electromagnetic fields penetrating narrow slots and lapped joints in thick conducting screens. *IEEE Transactions on Antennas and Propagation*, Vol. 36, No. 2, 1988, pp. 247-257.

[77] Craddock, I. J., Railton, C. J.: A new technique for the stable incorporation of static field solutions in the FDTD method for the analysis of thin wires and narrow strips. *IEEE Transactions on Microwave Theory and Techniques*, Vol. 46, No. 8, 1998, pp. 1091-1096.

[78] Douglas, M., Okoniewski, M., Stuchly, M. A.: Accurate modeling of thin-wire antennas in the FDTD method. *Microwave and Optical Technology Letters*, Vol. 21, No. 4, 1999, pp. 261-265.

[79] Mäkinen, R., Salonen, P., Kivikoski, M.: A new model for coupling a one-dimensional transmission line to FDTD grid for transient excitation of antennas. *Proceedings of the Asia-Pacific Microwave Conference*, Sydney, 2000, pp. 369-373.

[80] Hese, J. V., Zutter, D. D.: Modelling of discontinuities in general coaxial waveguide structures by the FDTD method. *IEEE Transactions on Microwave Theory and Techniques*, Vol. 40, No. 3, 1992, pp. 547-556.

[81] Maloney, J. G., Smith, G. S., Scott, W. R.: Accurate computation of the radiation from simple antennas using the finite-difference time-domain method. *IEEE Transactions on Antennas and Propagation*, Vol. 38, No. 7, 1990, pp. 1059-1068.

[82] Arlett, P. L., Bahrani, A. K., Zienkiewicz, O. C.: Application of finite elements to the solution of Helmholtz's equation. *Proceedings of the IEE*, Vol. 115, No. 12, 1968, pp. 1762-1766.

[83] Johnson, C.: *Numerical solution of partial differential equations by the finite element method*. Studentlitteratur, Lund, 1987, 279 p.

[84] Silvester, P. P., Ferrari, R. L.: *Finite Elements for Electrical Engineers*. Cambridge University Press, Cambridge, 1996, 494 p.

[85] Jin, J.: *The Finite Element Method in Electromagnetics*. Wiley-Interscience, New York, NY, 1993, 442 p.

[86] Nedelec, J. C.: Mixed finite elements in R^3. *Numerische Mathematik*, Vol. 35, 1980, pp. 315-341.

[87] Wong, S. H., Cendes, Z. J.: Combined finite element-modal solution of three-dimensional eddy current problems. *IEEE Transactions on Magnetics*, Vol. 24, No. 6, 1988, pp. 2685-2687.

[88] Bossavit, A., Mayergoyz, I.: Edge-elements for scattering problems. *IEEE Transactions on Magnetics*, Vol. 25, No. 4, 1989, pp. 2816-2821.

[89] Lee, J.-F., Sun, D.-K., Cendes, Z. J.: Full-wave analysis of dielectric waveguides using tangential vector finite elements. *IEEE Transactions on Microwave Theory and Techniques*, Vol. 38, No. 8, 1998, pp. 1262-1271.

[90] Cendes, Z. J.: Vector finite elements for electromagnetic field computation. *IEEE Transactions on Magnetics*, Vol. 27, No. 5, 1991, pp. 3958-3966.

[91] Fernandez, F. A., Lu, Y.: A variational finite element formulation for dielectric waveguides in terms of transverse magnetic fields. *IEEE Transactions on Magnetics*, Vol. 27, No. 5, 1991, pp. 3864-3867.

[92] Ledfelt, G., Edelvik, F., Andersson, U.: Hybrid time domain solver for the 3D Maxwell equations. *Proceedings of the Nordic Antenna Symposium Antenn 00*, Lund, Sweden, 2000, pp. 57-62.

[93] Taylor, R. L.: On completeness of shape functions for finite element analysis. *International Journal for Numerical Methods in Engineering*, Vol. 4, No. 1, 1972, pp. 17-22.

[94] Szabó, B. A., Babuška, I.: *Finite Element Analysis*. Wiley-Interscience, New York, NY, 1991, 368 p.

[95] Meixner, J.: The behavior of electromagnetic fields at edges. *IEEE Transactions on Antennas and Propagation*, Vol. AP-20, No. 4, 1972, pp. 442-446.

[96] Vafiadis, E., Sahalos, J. N.: Fields at the tip of an elliptic cone. *Proceedings of IEEE*, Vol. 72, No. 8, 1984, pp. 1089-1091.

[97] Van Bladel, J.: Field singularities at metal-dielectric wedges. *IEEE Transactions on Antennas and Propagation*, Vol. AP-33, No. 4, 1985, pp. 450-455.

[98] De Smedt, R., Van Bladel, J.: Field singularities at the tip of a metallic cone of arbitrary cross section. *IEEE Transactions on Antennas and Propagation*, Vol. AP-34, No. 7, 1986, pp. 865-870.

[99] De Smedt, R.: Electric singularity near the tip of a sharp cone. *IEEE Transactions on Antennas and Propagation*, Vol. 36, No. 1, 1988, pp. 152-155.

[100] Tracey, P., Cook, T.: Analysis of power type singularities using finite elements. International Journal for Numerical Methods in Engineering, Vol. 11, 1977, pp. 1225-1233.

[101] Pantic, Z., Mittra, R.: Quasi-TEM analysis of microwave transmission lines by the finite-element method. *IEEE Transactions on Microwave Theory and Techniques*, Vol. MTT-34, No. 11, 1986, pp. 1096-1103.

[102] Cendes, Z. J., Lee. J.-F.: The transfinite element method for modeling MMIC devices. *IEEE Transactions on Microwave Theory and Techniques*, Vol. 36, No. 12, 1988, pp. 1639-1649.

[103] Webb, J. P.: Finite element analysis of dispersion in waveguides with sharp metal edges. *IEEE Transactions on Microwave Theory and Techniques*, Vol. 36, No. 12, 1988, pp. 1819-1824.

[104] Gil, J. M., Zapata, J.: Efficient singular element for finite element analysis of quasi-TEM transmission lines and waveguides with sharp metal edges. *IEEE Transactions on Microwave Theory and Techniques,* Vol. 42, No. 1, 1994, pp. 92-98.

[105] Gil, J. M., Zapata, J.: A new scalar transition finite element for accurate analysis of waveguides with field singularities. *IEEE Transactions on Microwave Theory and Techniques,* Vol. 43, No. 8, 1995, pp. 1978-1982.

[106] Miniowitz, R., Webb, J. P.: Covariant-projection quadrilateral elements for the analysis of waveguides with sharp edges. *IEEE Transactions on Microwave Theory and Techniques,* Vol. 39, No. 3, 1991, pp. 501-505.

[107] Gil, J. M., Webb, J. P.: A new edge element for the modeling of field singularities in transmission lines and waveguides. *IEEE Transactions on Microwave Theory and Techniques,* Vol. 45, No. 12, 1997, pp. 2125-2130.

[108] Pantic-Tanner, Z., Savage, J. S., Tanner, D. R., Peterson, A. F.: Two-dimensional singular vector elements for finite-element analysis. *IEEE Transactions on Microwave Theory and Techniques,* Vol. 46, No. 2, 1998, pp. 178-184.

[109] Gordon, W. J.: Blending function methods of bivariate and multivariate interpolation and approximation. *SIAM Journal on Numerical Analysis*, Vol. 8, No. 1, 1971, pp. 158-177.

[110] Gordon, W. J., Hall, C. A.: Construction of curvilinear co-ordinate systems and applications to mesh generation. *International Journal for Numerical Methods in Engineering,* Vol. 7, No. 4, 1973, pp. 461-477.

[111] Gordon, W. J., Hall, C. A.: Transfinite element methods: blending function interpolation over arbitrary curved element domains. *Numerische Mathematik*, Vol. 21, No. 2, 1973, pp.109-129.

[112] Kärkkäinen, M.: *Use of finite-element method in the analysis of waveguides containing wedge singularities.* Diploma thesis (in Finnish), Helsinki University of Technology, 2000, 57 p.

HELSINKI UNIVERSITY OF TECHNOLOGY RADIO LABORATORY REPORTS

S 232 Hahkio, T.
Mapping of ILS Scatterers and Suppression of Scatter Errors, Oct. 1998

HELSINKI UNIVERSITY OF TECHNOLOGY RADIO LABORATORY REPORTS

S 233 Zhang, J.
Diode Modeling and Circuit Design of Microwave and Millimeter-wave Frequency Multipliers and Mixers, Dec. 1998

S 234 Heikkilä, E.
Tutkatekniikka, Feb. 1999

S 235 Heikkilä, E.
Tutkan signaalinkäsittely, Feb. 1999

S 236 Räisänen, A.V., Lindberg, S.
HUT Radio Laboratory Research and Education 1998, April 1999

S 237 Piironen, P.
Microwave Circuits and Systems for Space Applications, July 1999

S 238 Räisänen, A.V.
Opinnäytetyöt radiotekniikassa 1924-1999
Theses in Radio Engineering 1924-1999, July 1999

S 239 Sehm, T.
Development of Low-profile Radio Link Antennas for Millimeter Waves, Feb. 2000

S 240 Vainikainen, P., Ollikainen, J., Kivekäs, O., Kelander, I.
Effect of Phone Chassis on Handset Antenna Performance, March 2000

S 241 Räisänen, A.V., Lindberg, S.
HUT Radio Laboratory Research and Education 1999, April 2000

S 242 Lundén, O-P.
Low Noise Amplifiers and Local Oscillators for Wireless Communications Receivers, April 2000

S 243 Nyfors, E.
Cylindrical Microwave Resonator Sensors for Measuring Materials under Flow, April 2000

S 244 Kivinen, J.
Development of Wideband Radio Channel Measurements and Modeling Techniques for Future Radio Systems, March 2001

S 245 Räisänen, A.V., Lindberg S.
HUT Radio Laboratory Research and Education 2000, March 2001

S 246 Ala-Laurinaho, J.
Numerical Studies on a Radio Frequency Hologram and its Use in Antenna Measurements, May 2001

ISBN 951-22-5473-5
ISSN 1456-3835